A Study of Excited State Atoms in Cold Atom Traps and a test of the Reif Model to Determine Trap Depth

by

Nathan Evetts

A THESIS SUBMITTED IN PARTIAL FULFILLMENT OF
THE REQUIREMENTS FOR THE DEGREE OF

BACHELOR OF SCIENCE

in

The Faculty Science

(Physics)

THE UNIVERSITY OF BRITISH COLUMBIA

(Vancouver)

April 2011

Abstract

The motivation, theory and applications of atomic traps are briefly reviewed before delving into the primary motivation for the research: the disagreement between theory and experiment for the calculation of trap loss rate constants ($< \sigma v >$) for Rubidium Magneto-Optical Traps. We use a pure magnetic trap to calibrate for the density of background Rubidium in our system while varying this density and measuring the loss and loading rates for multiple magnetic traps for which the trap depth has been measured previously. This variation of density allows us to infer $< \sigma v >$, a quantity whose behaviour we attempt to explain in relation to the the excited state fraction of the trapped atoms. We find a strong correlation between the excited state fraction and the loss rate constant which we are, unfortunately, unable to quantify due to data quality issues. In addition to this study, experimental evidence for the confirmation of the Reif Model is provided as well as a new method (based on this model) for measuring the depth of a magneto-optical trap.

Preface

All theoretical predictions for $< \sigma v >$ were carried out by collaborators within the Quantum Degenerate Gas Laboratory at the University of British Columbia, principally by David Fagan and Dallas Clement.

Table of Contents

List of Tables

List of Figures

Acknowledgements

I would like to acknowledge a few people: Kirk Madison and James Booth, without whose help and encouragement this thesis surely would not be possible; Janelle Van Dongen whose enlightening input at the lab saved me hours of headache; and finally Calvin Childs, Paul Godin, and Dallas Clement, who lent their time to help take data.

Dedication

This is for all the Yaks out there.

Chapter 1

Introduction

1.1 Neutral Atom Traps

Neutral atom traps provide the ability to cool and confine atoms to millikelvin and submillikelvin temperatures. The resulting cloud of trapped atoms is typically about $10\,\mu$m - 5 mm in radius, containing up to 10^{10} atoms. The cooling and confining mechanisms require the use of optical and / or magnetic forces which are localized within a vacuum cell. The optical forces are implemented with lasers of a specific frequency and cause the atoms to absorb and emit photons, an effect which we exploit in order to measure their presence. Using a CCD camera, we image the cloud of cold trapped atoms as in figure 1.1.

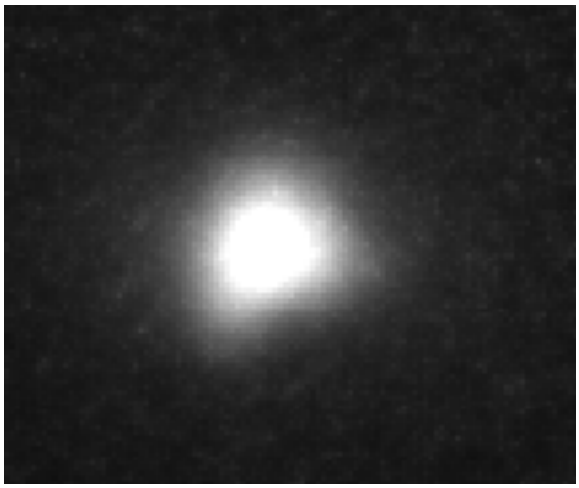

Figure 1.1: A picture of cold trapped atoms taken within the QDG lab at UBC. The atoms emit light because we are shining lasers on them which cause the absorption and emission of photons.

1.1.1 Magnetic traps

In the presence of a magnetic field our atom (which can be thought of as a magnetic dipole) will have an energy

$$E_B = -\vec{\mu} \cdot \vec{B} \tag{1.1}$$

where $\vec{\mu}$ is the magnetic moment of the atom and $\vec{B}$ is the applied magnetic field. Since we concoct a field such that $\vec{B_z} \propto z$, , $\vec{B_x} \propto x$, $\vec{B_y} \propto y$ (where $\vec{B_z}$, $\vec{B_x}$ and $\vec{B_y}$ are the z, x and y components of the magnetic field respectively) the lowest energy state for the atom is at $(x, y, z) = (0, 0, 0)$. This is the basis of the magnetic trapping force.

The trap can be considered a potential well of a certain depth (called the "Trap Depth", U) which is calculable according to

$$U = \mu r \nabla B_r \tag{1.2}$$

where r is the distance from the magnetic zero at $(0, 0, 0)$ to the wall of the vacuum cell and B_r is the magnetic field strength along either the $\hat{x}$, $\hat{y}$. Along the $\hat{z}$ axis the field gradient is different, and a the gravitational force on the atoms must be accounted for. Once an atom touches the wall of the vacuum it is instantly heated to room-temperature and will escape the trap.

This type of trap which uses only magnetic fields to confine the atoms is called a magnetic trap. It typically has exhibits a shallower potential well (a smaller trap depth) than with the addition of optical forces which would create what is called a magneto-optical trap.

1.1.2 Magneto-optical traps

By adding lasers of a specific frequency to a magnetic trap, we obtain a magneto-optical trap. With lasers of the correct frequency we may bombard our atoms with photons that have an energy mapping to some atomic energy level transition. Actually the lasers we use are "detuned" from this resonance - that is, the frequency is slightly too small to drive the desired energy level transition. This is illustrated diagrammatically in figure 1.2 where a few energy levels are drawn with a red arrow indicating the transition driven by the laser. Note that figure 1.2 does *not* show the detuning.

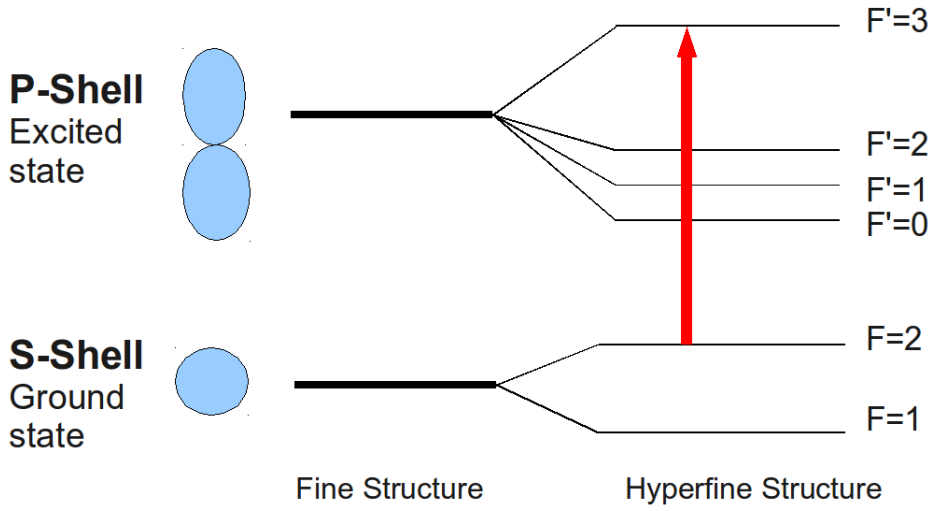

Figure 1.2: Some energy levels in ^{87}Rubidium. The red arrow indicates the energy of an incident photon driving the transition from energy eigenstates F=2 to F'=3. The detuning from has *not* been shown on this diagram. Childish depictions of the wavefunctions for each fine structure state are sketched in blue.

To obtain an optical trapping force we add a detuning to our lasers which then need to be set up in pairs which counter propagate. That is, we need two lasers pointing in opposite directions. This is illustrated in figure 1.3 where Rubidium atoms are drawn in black.

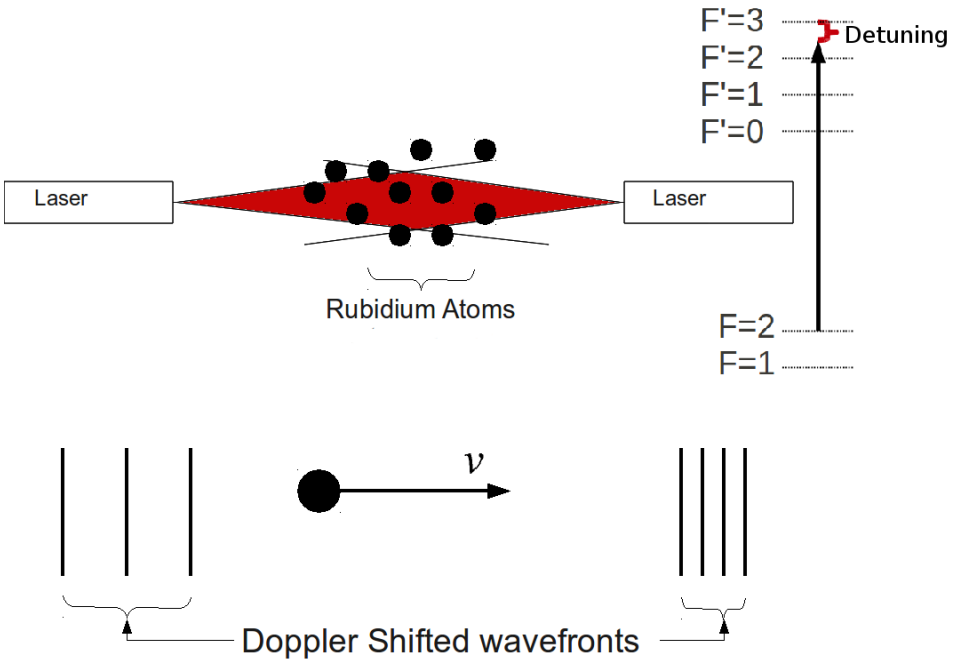

Figure 1.3: Two counter propagating lasers are aligned such that moving atoms doppler shift incoming photon frequency onto the resonance of an energy level transition thus causing the atom to absorb preferentially from the laser which acts to slow its motion.

A Rubidium atom traveling with some speed towards a laser will experience a doppler shift causing photons from one laser to have a higher frequency in the atom's frame, while photons from the other laser would have a lower frequency. Photons travelling in a direction opposite the atom will shift onto the resonance needed to drive an energy transition, while photons travelling in the same direction will shift away from this resonance. Therefore, the atom *preferentially absorbs photons which oppose its motion!*

If we align three of these laser pairs along the $\hat{x}$, $\hat{y}$ and $\hat{z}$ directions then we can confine the atom in three dimensions such that no matter which way the atoms move the lasers act to slow them down thus obtaining an "optical molasses" which exists anywhere within the beam lines of the lasers. If the atoms are in the presence of a magnetic field their energy levels shift according to the Zeeman effect. Since the magnetic field experienced by the atom depends only (to first order) on its position, the detuning of our lasers becomes position dependant thus giving the trap a preferential location.

This is the basis of laser cooling, and the addition of such optical forces to a magnetic field defines the magneto-optical trap.

1.2 Motivation

Both understanding and applications of cold atom traps resulting from laser cooling and magnetic confinement have grown many fold since it was first shown that light could be used to cool and confine atoms to submillikelvin temperatures. This section will attempt to briefly outline some of the ways in which these methods have become valuable to science and technology.

1.2.1 Applications

Radiation pressures and magnetic potentials have been used in magneto-optic traps and pure magnetic traps to realized Bose-Einstein Condensates (BEC) in the laboratory and thus confirm long predicted quantum mechanical theories on bosons at low temperatures [1]. The BEC is a new, novel, excotic form of matter in which bosons become macroscopically degenerate in the ground state of some potential landscape. Their observation in the lab resulted in a nobel prize in 2001. Though they have no well defined applications at present, their nature is often likened to the widely applicable laser (which is comprised of many photons occupying the same state).

Atomic traps have also been scaled down in size to become an "atom chip". The atom chip uses nano-fabricated current carrying and charged wires to create microscopic magnetic potentials that trap atoms. The fact

that the trap has been scaled down in size greatly improves the portability of the device and opens up possibilities for a wide range of applications. For example, in matter wave optics the versatility of the atomic chip has been likened to that of the integrated circuit in electronics [8].

The atom chip has even been scaled small enough to produce many particle entangled states and thus become a candidate for quantum quibits. The ability of the chip to create microscopic potentials for different atomic states provides distinction between the quibit $|0\rangle$ and $|1\rangle$ states. Atoms in a quantum superposition of states can be trapped in two separate potential wells. The chip's potential landscape can be modified to connect and disconnect these two wells in order for one quantum state to interact (or not) with the other. The interaction is thought to be able to produce a two quibit gate with the truth-table-like properties necessary for quantum computing. [3]

Yet another application of the atomic trap is found in the atomic clock. Atomic clocks utilize trapped and cooled atoms to electronically link regular time keeping crystal oscillators to the frequency of an atomic transition [4] [6]. Since a time interval (like a second) can be mapped to an exact number of cycles for some oscillator (like a quartz crystal) the oscillator is able to keep accurate time. The accuracy of a measured time interval depends on the reliability of the oscillator. Since crystal oscillations depend in part on environmental conditions, stabilizing the crystal's time keeping frequency with the atomic transition frequency can provide a clock accurate to $10^{-12}\%$.

All of these applications: BEC's , atom chips, atomic clocks and quantum gates utilize magnetic or magneto-optic trapping. Yet all traps experience loss: atoms which escape the trap. Escape occurs for a number of reasons which should be understood in order to properly utilize the trap for any given purpose. Such understanding will likely yield new applications. A recent example exists within our lab in the form of a patent for a new type of pressure sensor which infers pressure in a gaseous environment by measuring the loss of cold atoms in the trap due to collisions with the hotter surrounding gas.

1.2.2 Loss Rates from Magneto-optical Traps

Since the loss of atoms from a trap can effect the performance of any device which depends on this technology, it is important that we understand and be able to quantify this loss. Atoms are lost from the trap for a number of reasons. Trap loss can occur when:

1. Hot atoms in the vacuum cell collide with cold atoms in the trap.
2. Two cold atoms collide within the trap causing an energy transfer greater than the trap depth thereby ejecting one of the atoms
3. Two cold atoms and a photon converge in a three body collision which ejects one or both of the atoms from the trap.
4. An inelastic collision occurs where some internal atomic energy is transformed into kinetic energy, or where the atomic state changes to something no longer trappable.

In most cases (particularly at high densities), the dominate loss mode is the collision of cold atoms with hot atoms. If this is true we can define a collisional "loss rate constant", or "cross section for trap loss" $< \sigma v >$ which characterizes the fundamental interactions between the hot and cold atoms which are able to cause loss from the trap. Actually $< \sigma v >$ is a velocity averaged cross section for interaction. It represents the cross sectional volume for atomic interaction (since σ is a characteristic area and v is the velocity of the particle). The quantity σv is averaged over the Maxwell-Boltzmann distribution to obtain $< \sigma v >$ in units of volume / time. If the density profile of the cold atom trap is such that there exist atoms within this characteristic volume, then those atoms are ejected from the trap. The volume is calculated in such a way that collisions which do not impart enough energy to eject atoms from the trap are not included [19]. See figure 1.4 for a sketch of this process.

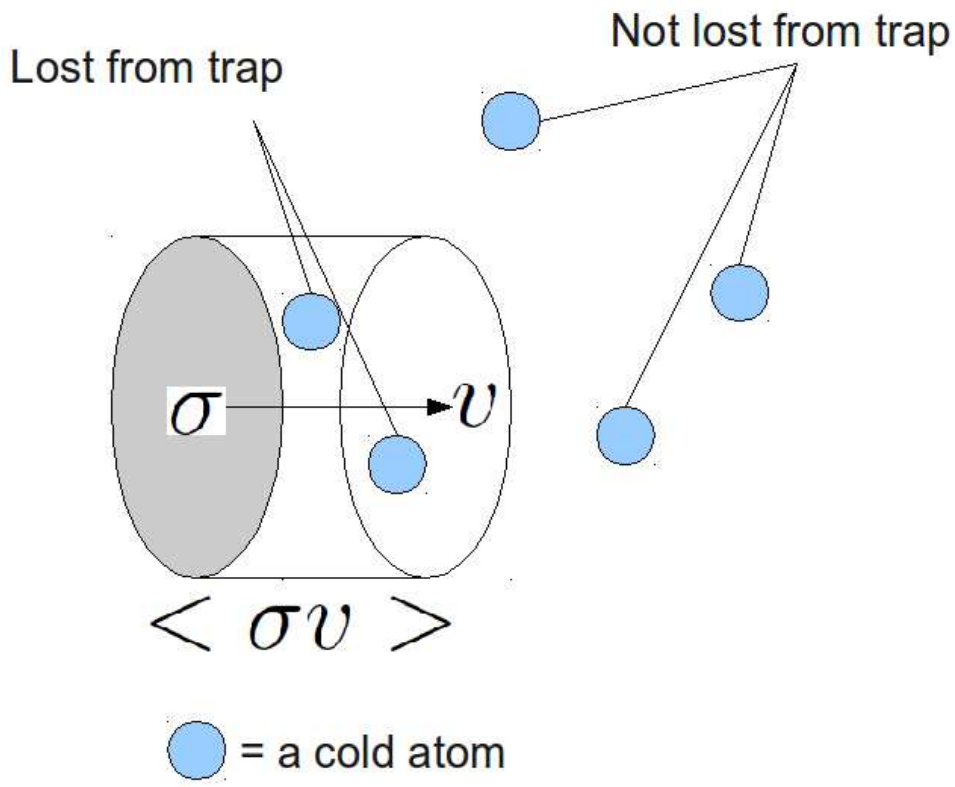

Figure 1.4: A pictorial interpretation of $< \sigma v >$, the cross section for trap loss.

In the past, $< \sigma v >$ was thought to depend almost entirely on the trap depth (U). A theoretical curve relates these two quantities in figure 1.5. The curve is calculated by numerically solving the Schrödinger equation with an interatomic potential called a Lennard-Jones Potential. Lennard-Jones potentials are models of the potential landscape which an atom feels as a result of another nearby atom, and are functions of distance between these two atoms. This method for determining is $< \sigma v >$ best outlined in [7]. Typical Lennard Jones potentials are seen in figure 1.7.

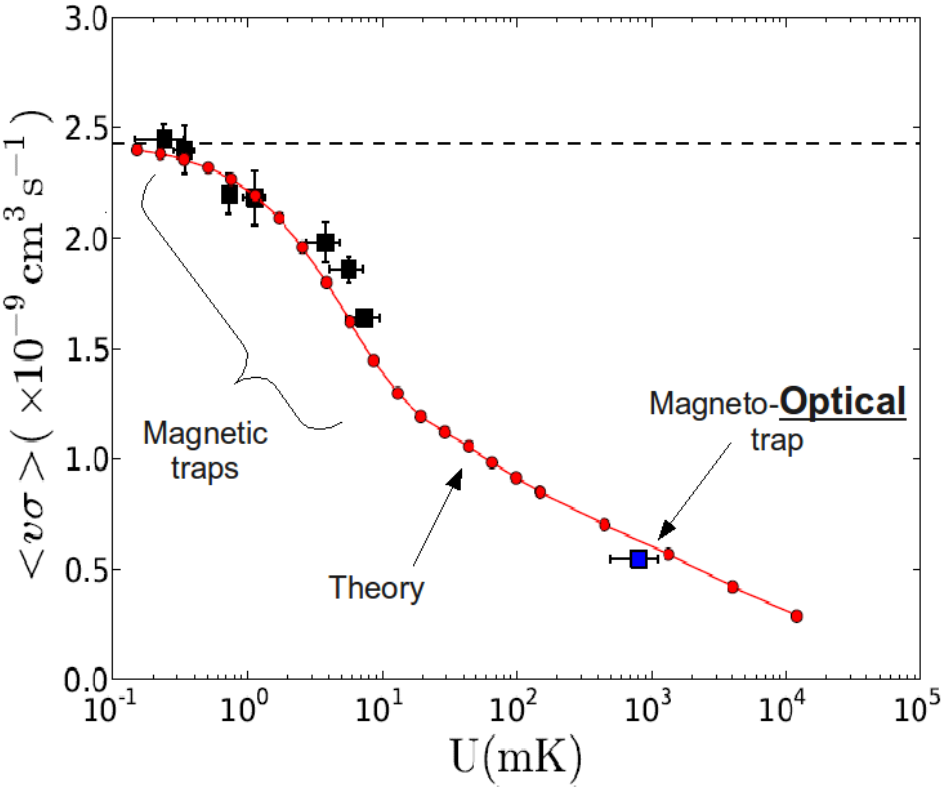

Figure 1.5: Our Theorectical model of the dependence of $< \sigma v >$ on trap depth U is plotted in red. Data corroborating the theory is in black (magnetic traps) and blue (magneto-optical traps). Figure from [7]

In figure 1.5 we trap Rubidium atoms and introduce some Argon into the vacuum cell which acts as our hot background gas and causes trap loss. We may measure the cross section $< \sigma v >$ and the Trap Depth U in order to compare with our predictions. In this case the theory and data are well matched. However, when we conduct the same experiment without any Argon, and with only Rubidium acting as the hot background gas, something puzzling happens. The measured $< \sigma v >$ agrees with the prediction when we trap atoms magnetically, however, once we change to a magneto-optical trap, we see pronounced disagreement (see figure 1.6).

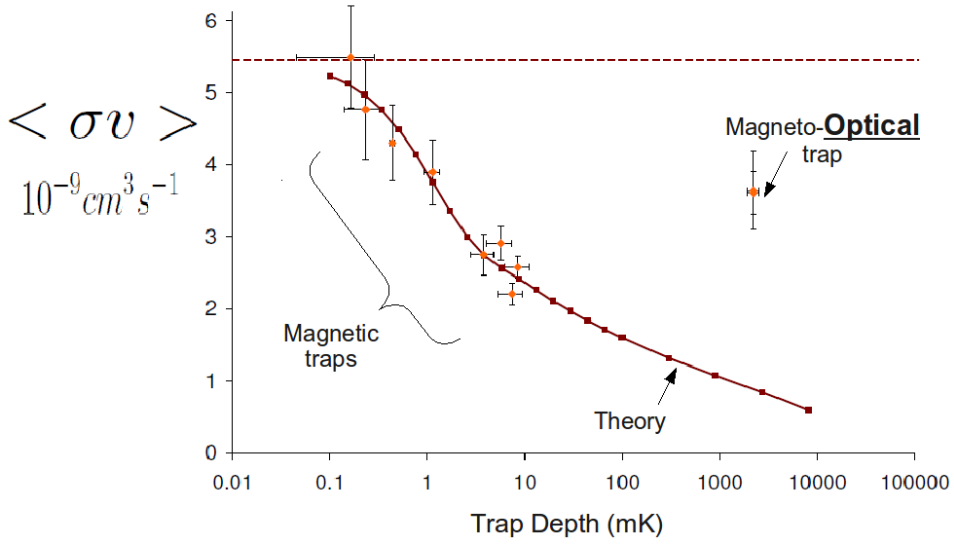

Figure 1.6: Our Theorectical model of the dependence of $< \sigma v >$ on trap depth U is plotted in red. This time there is no Argon but only Rubidium acting as a hot background gas. The theory (dark red) matches for the magnetic traps, but fails for the magneto-optical one. Figure from [19]

In attempting to explain this disagreement, we note the main difference between the magnetic and magneto-optical trap is the presence resonant laser light. This light causes some fraction of the atoms to exist in an excited state. It should not be hard to believe that such states would have significant effects on the trap loss. Intuitively one expects the interaction between an excited state and a ground state atom should be different from that between two ground state atoms just from inspection of the shapes

of their wavefunctions (see figure 1.2). Further this difference is quantified by the interatomic Lennard Jones potentials which are different for ground-ground state interactions versus ground-excited state interactions (see figure 1.7). The ground-excited interactions take a different, stronger form that has a longer range. This longer rage potential would suggest a higher interaction rate, and thus a larger cross section for trap loss than predicted in by the curves in figures 1.5 and 1.6 which are calculated using the ground-ground state potential.

In light of all this, the following thesis is intended to investigate trap loss dependence on excited state atoms in the hope of explaining the anomalous magneto-optical trap data in figure 1.6.

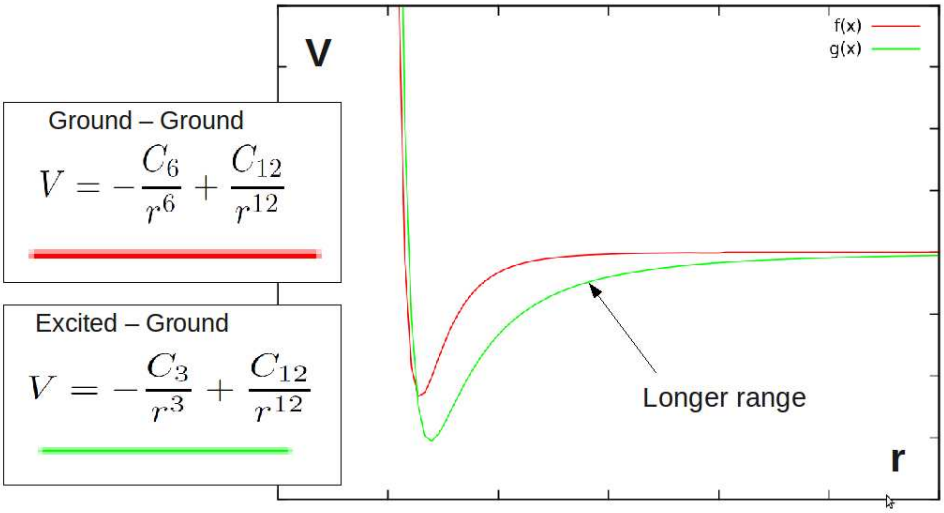

Figure 1.7: Typical lennard jones potentials for interactions between two ground state atoms (red) as well as for a ground and excited state interaction (green).

Chapter 2

Theory

2.1 Neutral Atom trap overview

2.2 Atomic Energy Levels: ^{85}Rb and ^{87}Rb

We model ^{85}Rb and ^{87}Rb as two level atoms where excited states are determined first by the orbital angular momentum and then by further hyperfine structure corrections. This experiment will involve transitions between $5^2S_{1/2} \rightarrow 5^2P_{3/2}$. This labelling convention denotes the energy level of the outermost electron bound to the atom. An energy level X^yP_z informs the reader that the principle quantum number is X, $Y = 2s + 1$ is the electron spin degeneracy, and $Z = J$ where J is the total electronic angular momentum $\vec{J} = \vec{S} + \vec{L}$ and $\vec{L}$ is the orbital angular momentum. The letters P and S correspond to different$\vec{L}$ states ($S \rightarrow L = 0$, $P \rightarrow L = 1$).

This convention is sufficient for what is called the "Fine Structure" of an atom.

As in typical quantum mechanics texts [9], the time-independant Hamiltonian

$$H\psi = E\psi \tag{2.1}$$

where $H = -i\hbar\nabla^2 - \frac{e^2}{4\pi\epsilon_o}\frac{1}{r^2}$, yields a spectrum of allowed energy levels for the bound electron. Adding a perturbation for spin-orbit coupling $H_{SO} = -\vec{\mu} \cdot \vec{B}$ and relativistic effects $H_{rel} = -\frac{p^4}{8m^3c^2}$ [9], where $\vec{\mu}$ is magnetic dipole moment of the electron, $\vec{B}$ is the effective magnetic field which it experiences, p is the standard momentum operator, m is the mass of the electron and c is the speed of light. Perturbation theory tells us that different states of the same principle quantum number (n) can split to different energy levels. A Rubidium atom (with $n = 5$) could theoretically be composed of a superposition of $L = 0$ and $L = 1$ states.

This description holds only to a certain precision. If we consider an even smaller perturbation to the Hamiltonian, we see further splittings in the allowed energy levels. This is called "Hyperfine structure". The new perturbation results from the interaction between the nucleus and the electrons. The nuclear angular momentum, I, couples to J. The same rules as before apply for addition of angular momentum. With

$$\vec{F} = \vec{J} + \vec{I} \tag{2.2}$$

we obtain energy eigenstates according to the quantum number F. Also important to note is the $2F + 1$ degeneracy inherent in each F state which results from the different possible projections of $\vec{F}$ along a particular axis (usually, by convention, the z-axis). For example, if $F = 2$ the $2F + 1 = 5$ states correspond to projections denoted $m_F = -2, -1, 0, +1, +2$.

More detailed theoretical consideration of the hyperfine corrections to the hamiltonian resulting energy levels can be found in [17],[16] and [2].

Some of these atomic states are sketched for ^{85}Rb in figure 2.1.

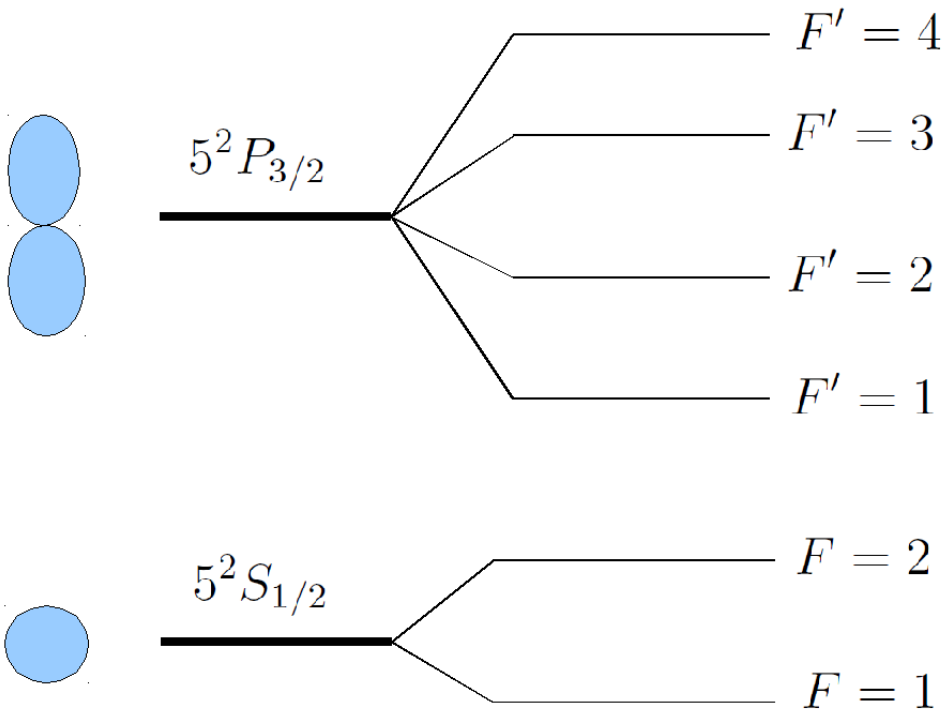

Figure 2.1: A sketch (not to scale) of both the fine and hyperfine energy levels in a ^{85}Rb atom . The $5^2P_{1/2}$ states have been omitted. Childish depcitions of the corresponding wavefunctions are drawn in blue.

With knowledge of these energy levels in hand, lasers of the correct frequency can be used to excite atoms from lower to higher energy states, thus producing the desired cooling force.

2.3 Scattering Rate and The Excited State Fraction

A steady state solution to the Optical Bloch equations [11] yields an expression for the fraction of atoms in an excited state ,f_e.

$$f_e = \frac{\Omega/\Gamma}{1 + 4(\Delta/\Gamma)^2 + 2(\Omega/\Gamma)^2} \tag{2.3}$$

Where Ω is the Rabi-frequency, Δ is the detuning from resonance, and Γ is the natural decay rate from the excited state. We then define the saturation intensity by

$$\frac{I}{I_{sat}} = 2\left(\frac{\Omega}{\Gamma}\right)^2. \tag{2.4}$$

and therefore

$$I_{sat} = \frac{c\epsilon_o\Gamma^2\hbar^2}{4|\hat{\epsilon}\cdot\vec{d}|^2} \tag{2.5}$$

where ϵ_o is the permittivity of free space, $\hat{\epsilon}$ is the unit vector of the light field and $\vec{d}$ is the dipole moment of the atom. The Rabi - frequency can be defined $\Omega = -\vec{d}\cdot\vec{E_o}/\hbar$ where $\vec{E_o}$ is the electric field resulting from resonant lasers. In general the expression for the saturation intensity is more complicated but in the case of circularly polarized light it reduces to

$$I_{sat} = \frac{\hbar\omega^3\Gamma}{12\pi c^2} \tag{2.6}$$

and the equation for for the fraction of atoms in an excited state can be written

$$f_e = \frac{1}{2}\frac{I/I_{sat}}{1 + 4(\Delta/\Gamma)^2 + (I/I_{sat})} \tag{2.7}$$

Another related quantity worth knowing is the scattering rate. The scattering rate is the rate at which photons are emitted from a population of trapped atoms. This is simply the fraction of excited atoms times the

rate (Γ) at which they decay to a ground state. Therefore the scattering rate is $R_s = \Gamma f_e$, or

$$R_s = \frac{\Gamma}{2} \frac{I/I_{sat}}{1 + 4(\Delta/\Gamma)^2 + (I/I_{sat})} \tag{2.8}$$

Equations 2.3 - 2.8 can be found in [17]

2.4 Cooling forces in MOTs and magnetic traps

The force on a atom results from the bombardment of photons and the momentum transfer which must therefore result. Since we align two counter-propagating beams we would expect that the forces would be equal and opposite, thus cancelling each other. However, since the atoms are moving with some velocity within a magnetic field, we must also consider both the Doppler and Zeeman effects which will effect detuning from resonance for each laser in the frame of the atom.

The force experienced by the atom is the net momentum transfer per photon per time [7]

$$\vec{F} = \hbar \vec{k} R_s \tag{2.9}$$

where $\hbar$ is plank's constant divided by 2π, $\vec{k}$ is the wave-vector of the photon and R_s is the scattering rate from equation 2.8.

Atomic motion causes a doppler shift which will cause the laser detuning from resonance to change by $\vec{k} \cdot \vec{v}$, where $\vec{v}$ is the velocity of the atom.

The magnetic field causes a spatially dependent Zeeman shift. This causes photons to shift further from resonance by [12] $(g_e m_e - g_g m_g)\mu_B B/\hbar$ where g is the Lande-g factor, μ_B is the Bohr magneton, m is projection of the total angular momentum along the magnetic field and the subscripts e and g denote the excited and ground states respectively.

The overall effective detuning from resonance experienced by the atom is therefore

$$\Delta_{eff} = \Delta + \vec{k} \cdot \vec{v} + (g_e m_e - g_g m_g)\mu_B B/\hbar \tag{2.10}$$

Putting these effects together yields an expression for the force exerted on the atom by one laser

$$\vec{F} = \hbar \vec{k} \frac{\gamma}{2} \frac{I/I_{sat}}{1 + 4(\Delta_{eff}/\Gamma)^2 + (I/I_{sat})} \tag{2.11}$$

Note that the net force must consider the sum resulting from lasers propagating in both the "+" and "-" directions: $\vec{F_{net}} = \vec{F_+} + \vec{F_-}$.

Next we consider the cooling force present in the purely magnetic trap. This force is much simpler to calculate and results from the atomic tendency towards lower energy configurations. The change in the atomic energy due to the Zeeman effect is

$$\Delta E_z = \mu_B g_F m_F B \tag{2.12}$$

Since our coil configuration produces a roughly linear magnetic field, we may re-write this equation

$$\Delta E_z = \mu_B g_F m_F \frac{dB}{dz} z \tag{2.13}$$

where z is the cartesian coordinate. Therefore the resulting magnetic force is

$$F = -\mu_B g_F m_F \frac{dB}{dz}. \tag{2.14}$$

Of note is that this type of trap will necessarily have both high and low field seeking states depending on the sign of $g_F m_F$. Since our coil system has a field zero at its centre, we call low field seeking states, "trappable", while the others are "untrappable".

2.5 Rate Equations

2.5.1 Elastic Collisions

The equation which governs the number of atoms (N) confined to a given trap is [12]

$$\frac{dN}{dt} = R - \Gamma N - \beta \int n^2 \, \mathrm{d}V \tag{2.15}$$

Where R is the rate at which atoms are loaded into the trap, n is the density of trapped atoms and V is the volume which the trap occupies. The loss rate coefficients (Γ and β) are each representative of trap loss via different mechanisms. Γ is a term representing a decrease in N due to collisions between hot background atoms and cold trapped ones. Typical MOT's are created in a high vaccum cell where the densities are very low so that optical

and magnetic cooling forces can act undisturbed by comparatively high density, high temperature conditions which would destroy any confined cloud of cold trapped atoms. When, however, an atom comes into contact with the vacuum wall it is nearly instantaneously heated to room-temperature. When such atoms collide with cold trapped atoms the trap experiences atom loss. These are the types of losses described by the Γ term in equation 2.15.

More fundamental than the loss rate, Γ, is the cross section for trap loss, $< \sigma v >$. The two are related by

$$\Gamma = \sum_a n_a < \sigma v >_a \tag{2.16}$$

where n_a is the density of a background gas "a" and $< \sigma v >_a$ is the cross section for trap loss that considers interactions between species "a" and the trapped species. As illustrated in figure 1.4 $< \sigma v >_a$ represents a likelihood for interaction between two atoms resulting in trap loss.

Also possible are cold collisions between trapped atoms as well as light assisted collisions, where a photon and two cold atoms scatter via a three - body collision. Either of these collisions could cause an energy transfer which would raise an atom's energy above the "trap-depth" (ie: the maximum trappable energy) thus causing this atom to be lost from the trap. β is multiplied by the integral of n^2 over the entire volume of the trap inorder to account for the fact that collisions between trapped atoms should scale like the probability of one atom interacting with another $(n \cdot n)$. The terms in equation 2.15 are illustrated pictorially in figure 2.2.

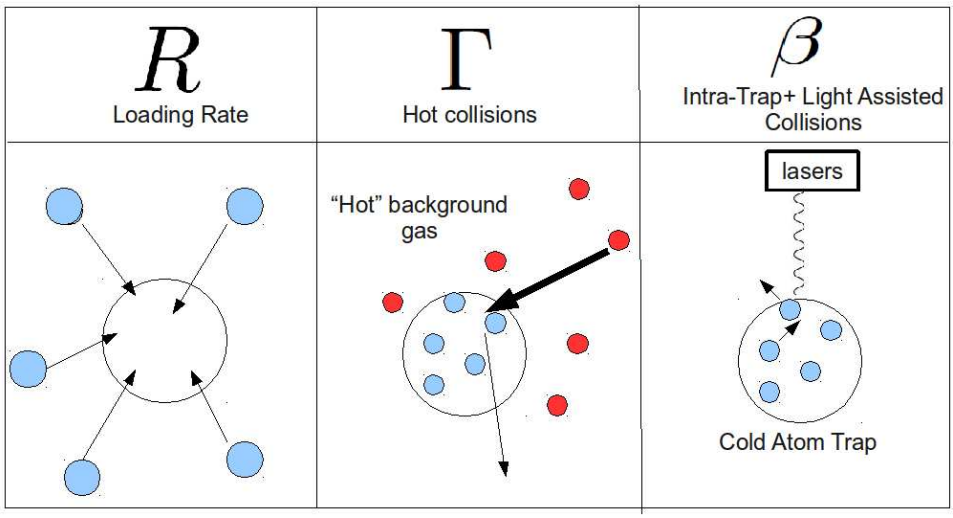

Figure 2.2: Coefficients from equation 2.15 are summarized graphically

2.5.2 Inelastic Collisions

The previous section discussed collisions in which the internal energy of the participants did not change between their initial and final states. However, other sources of trap loss can be found via collisions which do just that. Two models for this type of loss were put forward by Gallagher and Pritcher in 1989 [18]. Their semi-classical picture involved one of two atoms absorbing a photon causing the pair to enter an excited molecular state where the atoms are bound to eachother via dipole interactions described by potential wells like that of figure 2.3. In an optical trap the absorption of a photon drives the transition $S_{1/2} \rightarrow P_{3/2}$. One of two different things may then happen to the molecule to transform internal energy into the kinetic energy necessary for an atom to escape its trap. Firstly a fine structure change can occur, $P_{3/2} \rightarrow P_{1/2}$, releasing an energy, ΔE_{FCC}, to be equally divided between the two atoms. In the case of Rubidium $\Delta E_{FCC}/h \simeq 7\text{THz} \simeq \frac{4.6\times10^{-21}\text{J}}{k_B} \simeq 340\text{K}$ (where h and k_B are Plank's and Boltzmann's constants respectively) which is much greater than the typical MOT trap depths of $\simeq 2\text{K}$.
Radiative escape is another form of inelastic collision. An excited molecular pair of the form $S_{1/2} + P_{3/2}$ may traverse the potential landscape of figure 2.3 towards the lower energy regions of the potential well. If the molecule releases less energy by photon emission in its decay that was absorbed in its excitation, the remaining energy is transformed into kinetic energy and may then be carried away by the atoms. That is:

$$S_{1/2} + S_{1/2} + \hbar\omega \rightarrow S_{1/2} + P_{3/2} \rightarrow S_{1/2} + S_{1/2} + \hbar\omega' \tag{2.17}$$

where $\omega > \omega'$ and the atoms each gain kinetic energy $\hbar(\omega - \omega')/2$.

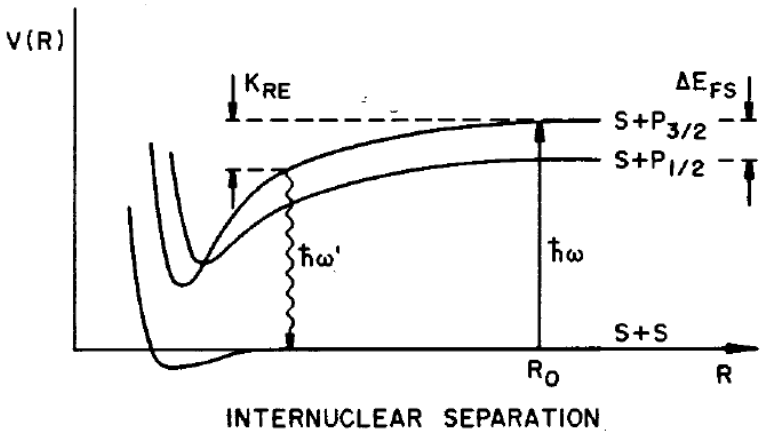

Figure 2.3: Possible paths take by atoms in a molecular state through an energy phase space. Radiative escape occurs when the molecular pair of atoms rolls into a potential well and then emits a photon of a lower energy than it absorbed inorder to reach that molecular state. The difference in energy is carried away by the atoms which could then escape the trap. Fine structure changing collisions occur when one atom falls from the $P_{3/2}$ state to the $P_{1/2}$ state. Again the difference in energy is carried away by the atoms. Figure from [18].

2.6 The Reif Model for loading rates and trap depth

Reif models the flux of particles, dN/dt, through a surface, dA, [15]

$$dN = f(v)v\cos(\theta)dtdA\,d^3v \tag{2.18}$$

where $f(v)$ is the maxwell boltzman distribution

$$f(v)d^3v = \left(\frac{m}{2\pi k_B T}\right)^{3/2} e^{-\frac{mv^2}{2k_B T}} v^2 \sin(\theta)dvd\theta d\phi \tag{2.19}$$

θ and ϕ are the usual spherical coordinates , v is the velocity of the particle, k_B is the Boltzmann constant, T is the temperature of the particles and m is their mass.

From this, applying the logic of [13], we may derive a model for the Loading rate R which depends on the MOT capture velocity v_c, or possibly the trap depth U.

Knowing that atoms below a velocity called the capture velocity (v_c) are captured by magnetic and optical forces we can integrate equation 2.18 from $v = 0$ to $v = v_c$ obtaining

$$R = \frac{dN}{dt} = \int_0^{v_c} f(v)d^3v\, v\cos(\theta)dtdA \tag{2.20}$$

$$R = \int_0^{v_c} \left(\frac{m}{2\pi k_B T}\right)^{3/2} e^{-\frac{mv^2}{2k_B T}} v^2 \sin(\theta)\, v\cos(\theta)dtdAdvd\theta d\phi. \tag{2.21}$$

Assuming that the capture velocity is low, we make the approximation that $\frac{mv^2}{2k_B T} \ll 1$ for the relevant region of the integral and substitute $e^{-\frac{mv^2}{2k_B T}} \simeq 1$ in equation 2.21 allowing us to evaluate the integral and obtain:

$$R = \frac{2An}{\pi^2 v_T^3} v_c^4 \tag{2.22}$$

where A is the cross sectional area of the trap, n is the density of particles and $v_T = \sqrt{\frac{8k_B T}{\pi m}}$.

If we want to incorporate the trap depth into this model for the loading rate, we can make the further approximation that

$$U = \frac{1}{2} m v_c^2 \tag{2.23}$$

and write

$$R = \frac{2An}{\pi^2 v_T^3} \frac{4U^2}{m^2}. \tag{2.24}$$

Of course the approximation in equation 2.23 is not strictly true. The trap depth should really be defined

$$U = \frac{1}{2} m v_e^2 \tag{2.25}$$

where v_e is the *escape* velocity. This is the velocity needed for a trapped atom to make it out of the trap, and is in principle different from that needed to trap an untrapped atom. Untrapped atoms can traverse the MOT area many times as they are bombarded with photons and spiral into the trap while trapped atoms only traverse this area once on their way out. This difference is illustrated in figure 2.4.

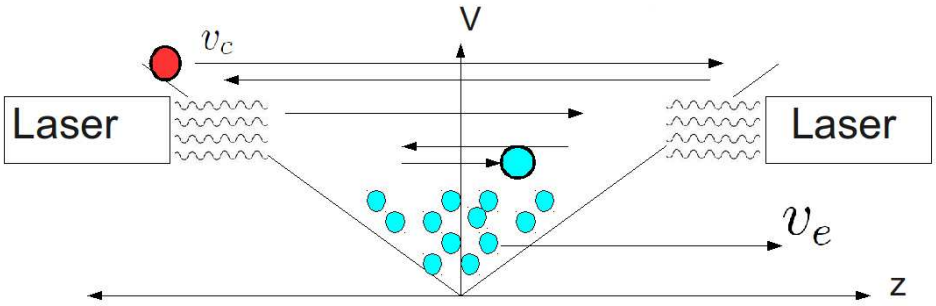

Figure 2.4: A hot (red) atom can traverse the trap many times experiencing continual bombardment of photons as it spirals into the trap, while a cold (blue) escaping particle only traverses this area once as leaves.

Chapter 3

Experiment

3.1 Experiment Set-up

The experimental set up of our apparatus is shown in figure 3.1.

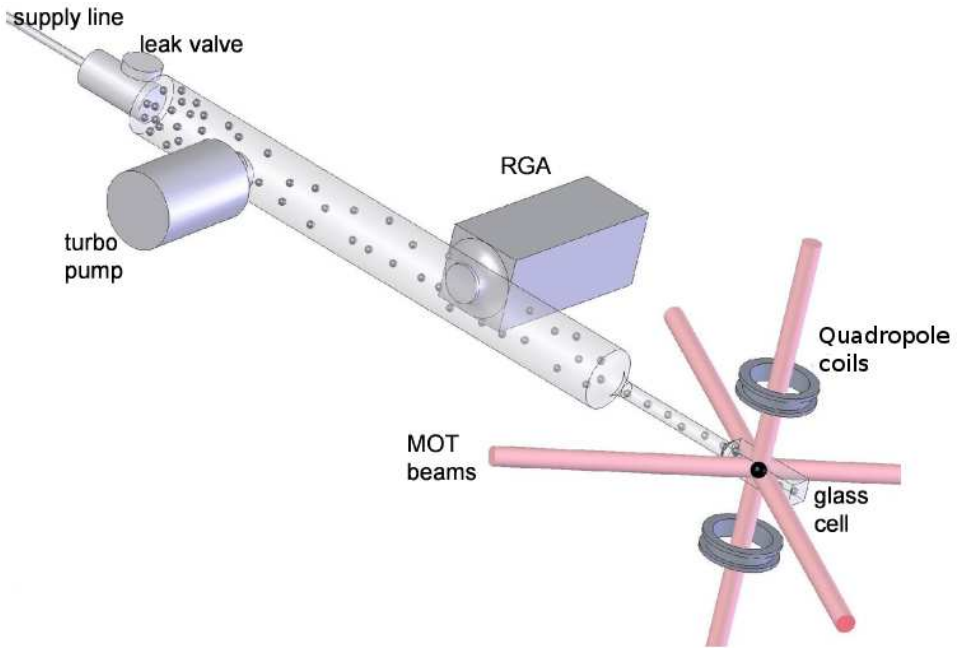

Figure 3.1: A sketch of our apparatus from [7]

A Rubidium dispenser introduces gaseous Rubidium to the a vacuum cell which is centred within a quadrupole coil system in anti-hemholtz coil configuration. Also centred on the cell are three pairs of two circularly polarized counter-propagating lasers.

The presence of trapped atoms is detected with a photodiode located behind a lens which focuses the light emitted from atoms as in figure 3.2

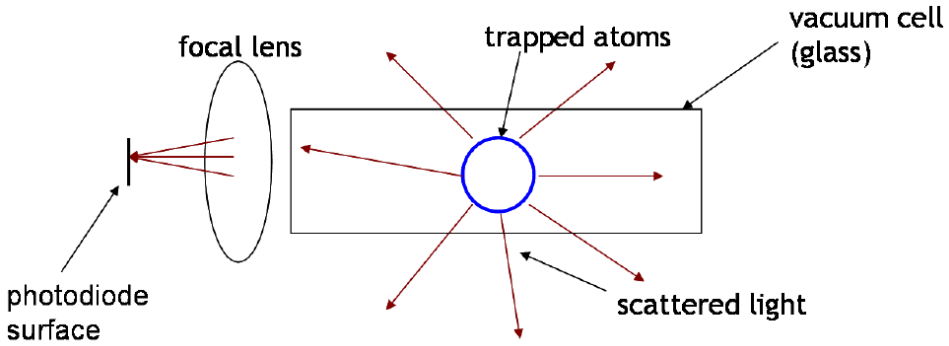

Figure 3.2: A diagram illustrating the detection of atomic florescence [7]

Given the picture in figure 3.2, one can calculate the power received by the photodiode as

$$P = h\nu \frac{r_{lens}^2}{d_{lens}^2} R_s N \tag{3.1}$$

where r_{lens}^2/d_{lens}^2 is the ratio of light hitting the lens from the spherically symmetric light emitted from the trap as calculated from the distance between the trap and the lens (d_{lens}) as well as the radius of the lens (r_{lens}). R_s is the scattering rate from equation 2.8, N is the number of trapped atoms, and $h\nu$ is the energy of the photon. Not accounted for here are power losses due to atomic florescence reflection at the walls of the glass vacuum cell.

A more detailed description of the laser systems can be found in [10]. Detailed description of the vacuum system and pumps, rubidium vapourizer, magnetic coils, and imaging systems (photodiode) can be found in [7] and [19].

3.2 Experiment Procedure

With the previously mentioned apparatus, we are ready to conduct our experiment. The procedure is as follows:

1. Fill Rubidium cell: At the beginning of a data run, a 5 Amp current is applied to a piece of Rubidium for roughly 2 - 3 minutes. This process is typically referred to as a "fill". The exact amount of time for

which the current is applied is not accurately measured as later calibrations will allow us to infer the density of Rubidium in our vacuum cell independent of the time for which this fill is preformed.

2. Wait approximately two hours for density levels to equilibrate. For sometime after the fill has been stopped Rubidium will continue to enter the system causing the density to rise on a time-scale that is comparable to that needed to take a density measurement ($\simeq$ 25 minutes). We therefore wait for the Rubidium density to stabilize and decay normally from some peak value before beginning to take data.

3. Having decided which trap parameters we wish to take data for, we proceed to take "loading curves". This means that we turn the MOT on with lasers at a specific detuning and intensity setting as well as with a specific current on our anti-helmholtz coils (which results in a desired magnetic field gradient). The trap parameters which we have studied so far are summarized in table 3.1.

Trap #	Detuning δ (MHz)	AOM setting	Intensity (mW/cm^2)	Trap Depth (K)	Magnetic field gradient (G/m)
1	12	0.8	34.5	2.2	2785
2	12	0.3	9.6	1.99	2785
3	12	0.27	6.9	1.8	2785
4	10	0.21	2.7	1.06	2785
5	10	0.3	9.6	1.1???	2785
6	8	0.21	2.7	0.92	2785
7	5	0.21	2.7	0.64	2785
8	8	0.21	2.7	0.92	2785

Table 3.1: A Summary parameters for different Magneto-optical traps for which we have taken data.

Once the MOT has been on for some time and reach an equilibrium state where the number of trapped atoms is no longer changing, the magnetic fields are turned off allowing almost all the atoms to leave the trap. After this the fields are turned back on and photodiode data is recorded on an oscilloscope as the trap fills up again. A typical loading curve can be seen in figure 3.3.

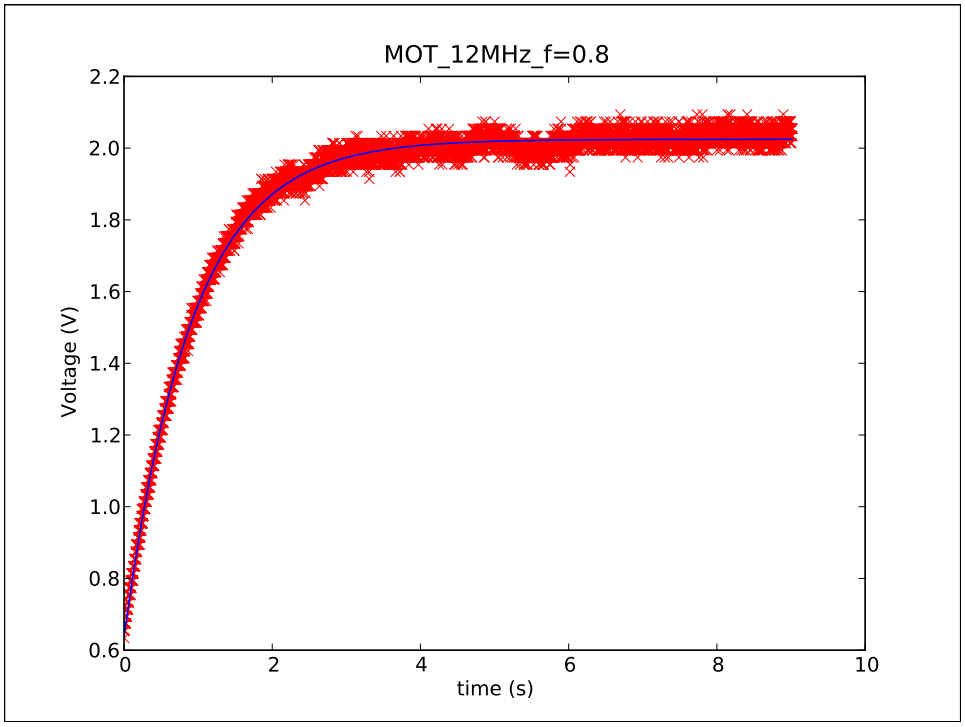

Figure 3.3: A typical loading curve for a Magneto-optical trap. This particular one has detuning $\delta = 12$ MHz and Intensity 34.5 mW/cm^2. The beginning portion of the trace which starts with a full trap and the drops abruptly (when the magnetic fields are turned off) has been cut from the plot.

We typically take five or six loading curves for three or four different MOTs before initiating a magnetic trap.

4. Initiate a magnetic trap. There is some greater difficulty in taking data for a magnetic trap since it requires that we turn our lasers off. This in turn means that our atoms are no longer absorbing and emitting photons and that we are unable to continuously measure the number of trapped atoms. In order to take such a measurement the lasers are flashed on for a short instant before being turned off again. The amount of light which we receive from the atoms as a result of the flash tells us how many atoms are in the trap. Unfortunately this method completely disturbs the evolution of the trap, which will no longer act as a purely magnetic trap. Therefore, each time a new measurement of trapped atoms is made it is necessary to create a new magnetic trap.

   We are interested in the loss rate of the magnetic trap. Because there is no light on, there is no loading term in equation 2.15 which can be simplified to

$$\frac{dN}{dt} = -\Gamma_{mt} N \tag{3.2}$$

   , an equation with an exponential solution $N = N_o e^{-\Gamma_{mt} t}$.

   A magnetic trap can be initialized by turning on a magneto-optical trap and then "dropping" our atoms into the purely magnetic trap by turning off the lasers and increasing the magnetic field strength. The lasers are kept off for some amount of time (called the hold-time) before they are flashed on quickly in order to take a measurement of the number of atoms in the trap. The process is then repeated for many different hold-times which allows us to record a set of data points of the form (N_i,t_i) with which we can fit to the exponential model of equation 3.2 and extract the magnetic trap loss rate Γ_{mt}.

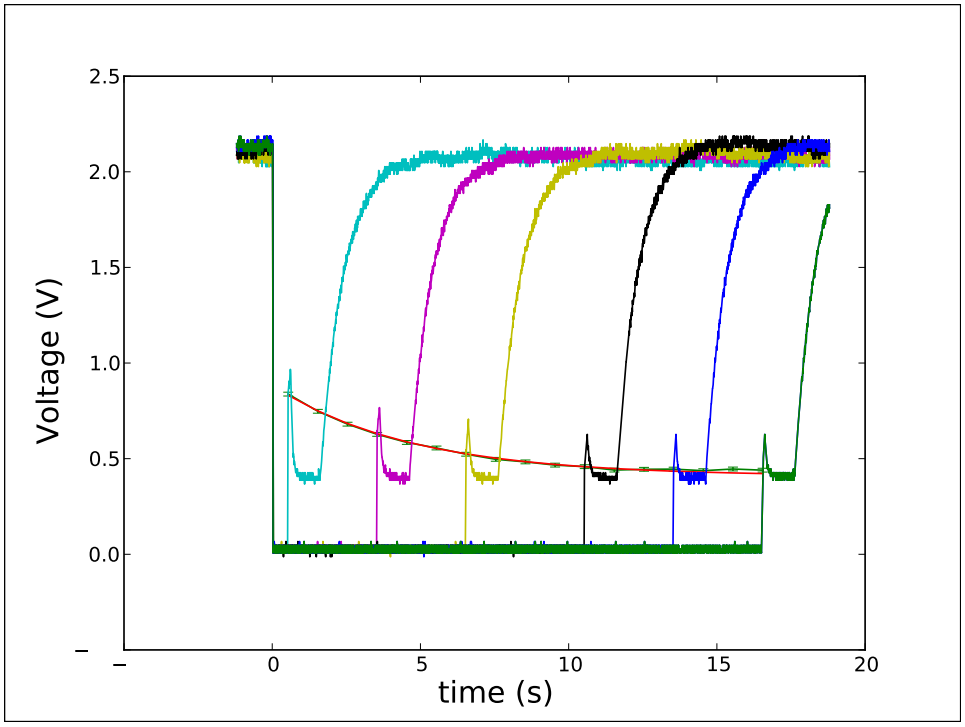

Figure 3.4: Multiple data curves for a magnetic trap are shown. The sharp spikes in the data correspond to the "flash" measurement conducted when the lasers are turned on. In red an exponential model has been fit to these points in order to determine the magnetic trap loss rate Γ_{mt}. After the "flash" measurement, the lasers are turned on again so that we can measure a load rate.

We also use the magnetic trap to measure the density of the hot background Rubidium in the vacuum cell, and so need to take a magneto-optical trap loading curve. Therefore, after this "flash" measurement of the number of atoms in the magnetic trap, we turn our magnetic fields off for one second to allow the trap to empty, before turning the lasers and fields on to a standard setting (Trap 1 from table 3.1) and measuring the load rate from the resulting curve. A few of these data curves are shown in figure 3.4 with the exponential fit to the "flash" measurements of the number of atoms in the magnetic trap overlaid.

Knowing from theory that both the magnetic trap loss rate Γ_{mt} and the loading rate R are proportional to the background density (n_{Rb}), we can use our knowledge of the depth of the magnetic trap to determine the relation between R and n_{Rb}.

In other words, since $\Gamma_{mt} =< \sigma v >_{mt} n_{Rb}$ and $R = k n_{Rb}$ a linear fit to the (Γ_{mt},R) data (as well as prior measurement of $< \sigma v >_{mt}$) will allow us to measure k. The linear relation of Γ_{mt} and R can be seen in figure 3.5. The magnetic trap therefore allows us to turn every measurement of R into a measurement of n_{Rb}, thus computing the density of background Rubidium in our vacuum cell. At the begining of a data run the cell is filled with Rubidium and allowed to decay. The decay of the density (as calculated by this method) is plotted in figure 3.6.

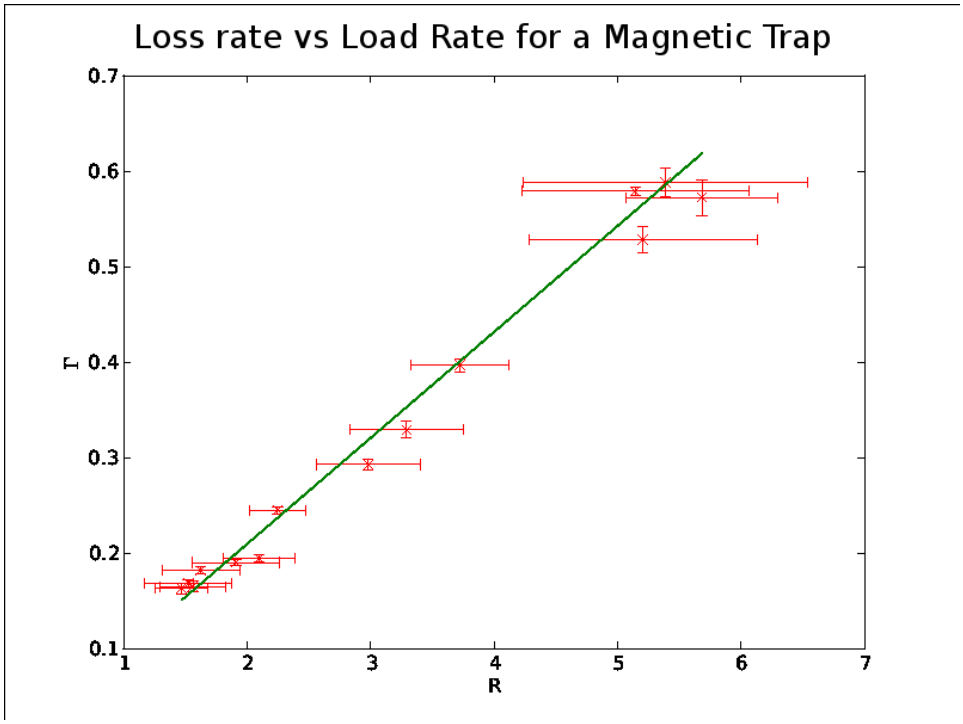

Figure 3.5: The loss rate for the magnetic trap Γ_{mt} is plotted against the loading rate, R, measured at the end of each data curve in figure 3.4.

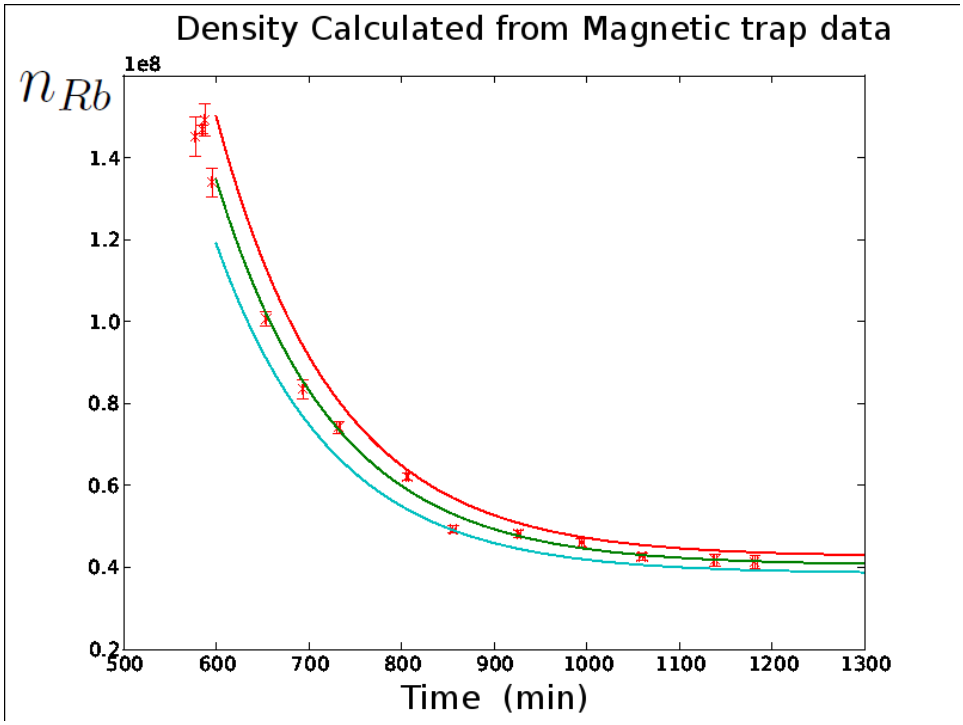

Figure 3.6: A plot of the density, calculated by the method of this section, is plotted versus time throughout a data run. At the beginning of the run we fill our vacuum cell with Rubidium and allow it to decay over the course of a day of data taking.

5. Having recorded the time of each n_{Rb} measurement , as well as the time at which each MOT loading curve is recorded, we interpolate n_{Rb} as a function of time and approximate the background Rubidium density at the time of each MOT loading curve.

   Making the approximation that

$$\Gamma N \ll \beta \int n^2 \, \mathrm{d}V \tag{3.3}$$

   and solving

$$\frac{dN}{dt} = R - \Gamma N \tag{3.4}$$

   as

$$N = N_o(1 - e^{-\Gamma t}) + b \tag{3.5}$$

   where $N_o = R/\Gamma$ is the steady state number of atoms trapped in the MOT, Γ is the loss rate due to hot background collisions, and b is a background term related primarily to laser reflections off the glass vacuum cell.

   We fit data as in figure 3.3 to the model in equation 3.5 in order to determine the loss rate Γ. Having already measured the density n_{Rb} with magnetic trap, and remembering that $\Gamma =< \sigma v > n_{Rb}$ we preform a linear fit to the (Γ,n_{Rb}) data in order to extract the cross section for trap loss (as in figure 3.7)

   Though the majority of Γ versus n_{Rb} graphs follow this trend, the linear relation is sometimes called into question with plots like figure 3.8 where the same data for another trap is plotted. This time a slight kink is observed at low densities.

   We preform these measurements on all of the traps in table 3.1.

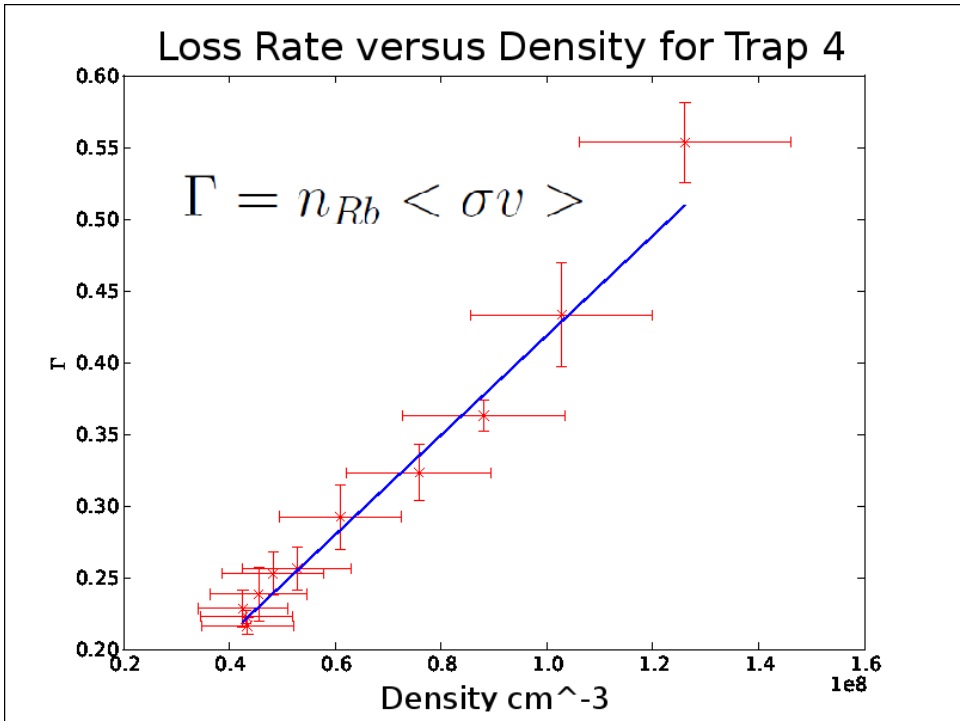

Figure 3.7: The loss rate for a magneto-optical trap (Γ) is determined by fitting data like in figure 3.3 to equation 3.5 and plotted versus the density n_{Rb}. The slope of a linear fit to this data gives us the cross section for trap loss $< \sigma v >$. This plot is for Trap 4, table 3.1.

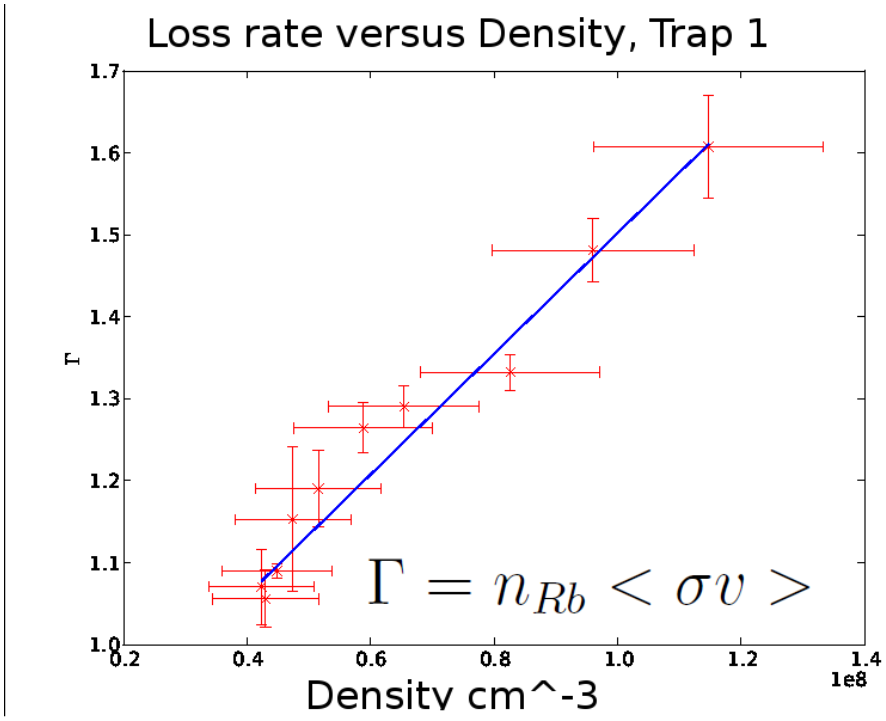

Figure 3.8: A suspicious kink is observed in this plot at low densities. The loss rate for a magneto-optical trap (Γ) is determined by fitting data like in figure 3.3 to equation 3.5 and plotted versus the density n_{Rb}. The slope of a linear fit to this data gives us the cross section for trap loss $< \sigma v >$. This plot is for Trap 1, table 3.1.

Chapter 4

Numerical Methods

4.1 Algorithm for fitting the Loading rate

In an attempt to determine the loading rate of a MOT one might take a trace like that in figure 3.3 and fit the data to equation 3.5 ($N = N_o(1 - e^{-\Gamma t}) + b$) thereafter employing the relation $R = \Gamma N_o$.

However, equation 3.5 does not actually satisfy the most general rate equation (equation 2.15, from which we have dropped the β term). We therefore attempt to determine the loading rate from a linear fit to the data for which there are few atoms in the MOT. In the limit $N \to 0$ equation 2.15 reduces to

$$N = Rt + b. \tag{4.1}$$

So a linear fit has the advantage of being applicable for any MOT, regardless of whether or not the approximation of equation 3.3 holds.

The most obvious problem with a linear fit is the question of how long the relation remains linear, and therefore: which data points should be considered in the fit? In the limit that $\Gamma t \ll 1$ we see that equation 3.5 also reduces to $N = Rt + b$. This requirement on Γt is essentially a restriction on how long we allow the MOT to load and therefore on how many atoms we allow in the trap before considering equation 4.1 invalid. But even now we have no exact boundaries for the region. The question has only become : how much less than 1 must Γt be for equation 4.1 to hold?

At first glance there is no obvious choice for the right amount of time, or the right number of points to be considered when preforming the fit. However, if one plots the value of R versus the number of points considered in the fit, as in figure 4.1, one observes large fluctuations in the value of R followed by stabilization and a steady decrease in the fit result for the loading rate. Actually figure 4.1 is plotted with the maximum Γt on the x-axis - that is, no points such that $\Gamma t > \Gamma t_{max}$ are considered in the fit.

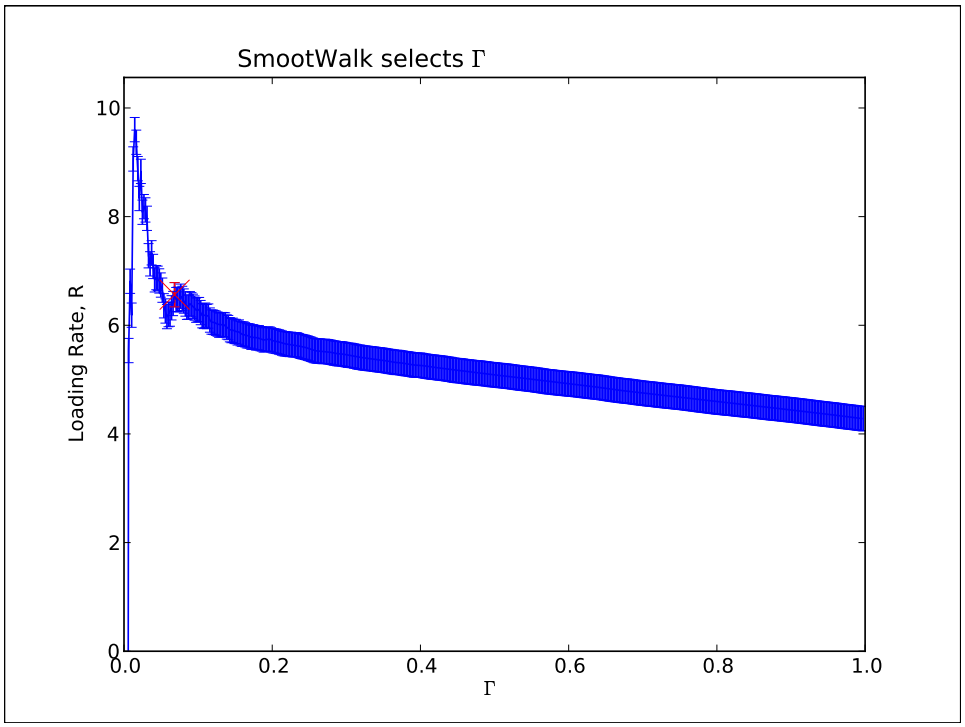

Figure 4.1: The loading rate R is determined from a linear fit to the first n points in the trace such that Γt is less than a certain value. This value is on the x-axis and ranges from 0 to 1. The red 'x' is the best R selected by the algorithm. In this particular case, n such that $\Gamma t < 0.068$ has been selected.

The wild fluctuations at small Γt_{max} map to too few points being considered in a fit which becomes dominated by noise and thus produces extreme values of R, typically with large errors. As the fit begins to consider larger and larger Γt_{max}, the value for R begins to decrease because the fit has considered points which are exhibiting the exponential nature of the data. The slope of the line is pulled down as the trace flattens out and tends towards a constant equilibrium value ($N_o + b$, from equation 3.5).

I consider that the best value for R is the highest value that is also stable. Intuitively, the most likely R should be the maximum one (the one which is least decreased due to effects of the exponential data) that is not dominated by noise in the data - noise which would produce a poor measurement of R.

This section is designed to present an algorithm which searches for this particular value of R - the maximum stable R - but the reader should note that I provide no quantitative test that this R is the correct one. The purpose of the algorithm will be to select a reasonable Γt_{max} which can be applied universally to traces for all MOTs in the hope that *consistency* will be achieved. That is, even if the R resulting from a linear fit to the first few points in a loading curve using some universal Γt_{max} is slightly wrong, the value will be systematically wrong by the same amount for each MOT.

The maximum stable R can be coherently searched for by first computing R based on a linear fit to the first n points in the loading curve such that $\Gamma t \leq 1$. By first fitting with this many points we guarantee that we overshoot the region in figure 4.1 where the value of R is noise dominated.

Call this value R_n, and remember its error, dR_n. These values will also be used to initialize the current "best" value for R: $R_n = R_{Best}$ and $dR_n = dR_{Best}$. Next preform the fit again, this time allowing consideration of only the first n-1 points. Call this value R_{n-1} with error dR_{n-1}. Next we want to check if this new value of R, which was computed by considering less points in the fit, has entered a region of large fluctuation indicative of noise dominated data.

If $R_{n-1} < R_{Best} + dR_{Best}$, $R_{n-1} > R_{Best} - dR_{Best}$ and $R_{n-1} > R_{Best}$, the algorithm interprets the value of R to have risen smoothly by considering one less point in the fit, and sets $R_{n-1} = R_{Best}$ and $dR_{n-1} = dR_{Best}$. Next the algorithm repeats this process with R_{n-2}, R_{n-3}...

The process continues until the latest value computed for R does not agree with R_{Best} within experimental error. That is, when considering R fit to some number of points i, $R_i > R_{Best} + dR_{Best}$ or $R_i < R_{Best} - dR_{Best}$. At this point the algorithm interprets the R to have entered a region of "too much fluctuation". Once this happens computation of R is complete and the last R_{Best} is the maximum stable R in the set.

Having preformed this algorithm on all of our MOT traces for data taken throughout this thesis, I find an average $\Gamma t_{max} = 0.18$. However, before obtaining this value, all computations of R were obtained by fitting with $\Gamma t_{max} = 0.1$. Future analyses might consider switching to $\Gamma t_{max} = 0.18$ and re-analysing past data.

4.2 Confirming the Reif Model and Measuring Trap Depth

Recall from the Reif Model that

$$R = \frac{2A}{\pi^2 v_T^3} n_{Rb} v_c^4 \tag{4.2}$$

or

$$R = \frac{8A}{\pi^2 v_T^3} \frac{U^2 n_{Rb}}{m_{Rb}^2} \tag{4.3}$$

where v_T is the mean velocity of the background gas, v_c is the capture velocity of the trap, m_{Rb} is the mass of the Rubidium atom and A is the cross sectional area of the MOT. In equation 4.3 we have made the substitution $U = \frac{1}{2} m_{Rb} v_c^2$.

We measure most of the quantities present in this model: R, n_{Rb} and sometimes (with more considerably more difficulty) U. (Note that R is calculated using the method of section 4.1 and by normalizing to the scattering rate from equation 2.8).

For a given apparatus alignment (which might effect A) and a given trapped species, I define the quantity

$$Q = \frac{R}{U^2 n_{Rb}} = \frac{2A}{\pi m_{Rb}^2 v_T^2} = \text{constant} \tag{4.4}$$

Next consider two different MOT's (i and j): one for which we know the trap depth U and one for which we do not. For any pair of measurements $(R_i, n_{Rb,i})$ and $(R_j, n_{Rb,j})$ we may couple data from the trap of known depth to the other and thereby measure the unknown depth. If Q is really a constant between the two traps then the logical question is: What U would scale the measurements of Q for the unknown trap so that they matched the known one as well as possible?

To answer this, I next consider

$$Q_i - Q_j = \frac{R_i}{U_i^2 n_{Rb,i}} - \frac{R_j}{U_j^2 n_{Rb,j}} = \frac{2\Delta A}{\pi m_{Rb}^2 v_T^2} \tag{4.5}$$

where ΔA is the difference in cross sectional area between the two MOTs. If we approximate $\Delta A \simeq 0$ then I can turn the determination of the unknown trap depth into a minimization problem. The function

$$S = \sum_i \sum_j (Q_i - Q_j)^2 = \sum_i \sum_j \left(\frac{R_i}{U_i^2 n_{Rb,i}} - \frac{R_j}{U_j^2 n_{Rb,j}} \right)^2 \tag{4.6}$$

couples every measurement of Q for one MOT (MOT i) to every other measurement of Q for the other MOT (MOT j). Letting U_j be a fit parameter and minimizing S produces a prediction for U_j.

In order to test this method, consider three traps for which separate measurements of the trap depth have already been made (Traps 1, 4 and 7 from table 3.1. To obtain results in table 4.1 I take Trap 7 to be the "known" trap, and test the method on Traps 1 and 4. The agreement is good, generally within 10 - 20 %.

Table 4.1: Comparing predictions for trap depth to previous measurement

MOT	Measured trap depth (K)	Fit Prediction (K)	percent difference
Trap 4	1.1	1.2 ± 0.05	8%
Trap 1	2.2	2.8 ± 0.14	21%

Since the capture velocity is typically higher than the escape velocity, we expect a slight overestimation of the trap depth.

Specifically, if $v_c \propto v_e$

$$v_c = k v_e \tag{4.7}$$

then separate measurement of the trap depth allows us to determine a value for $k = \sqrt{U_{fit}/U_{measured}}$. In the case of Trap 4 we get $k_4 = 1.04 \pm 0.6$ while for Trap 1 we see $k_1 = 1.13 \pm 0.03$, which agree within errors. Note that the errors on these k values are obtained only from considering error in the fit result for U and not from the independently measured values. So in the future trap depth corrections can be further corrected with this k factor.

But all of this is contingent on our trust in the Reif model. To check weather the value of Q is really constant, we plot many measurements of it throughout a data run (ie: for many different R and n_{Rb}). In figure 4.2 we normalize Q with the independently measured trap depths and in figure 4.3 with ones predicted by the minimization. Both plots exhibit a uniform, constant nature which suggests the Reif model is valid.

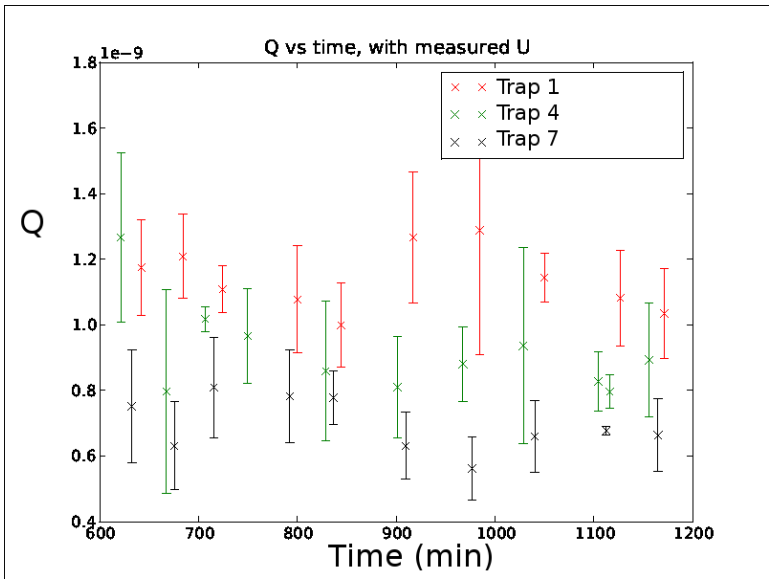

Figure 4.2: Q calculated with the independently measured trap depth is plotted for a particular data set (taken Feb 18, 2011). The roughly constant nature of the value for multiple measurements throughout the day (at different R and n_{Rb} regimes) points to a validation of the Reif model.

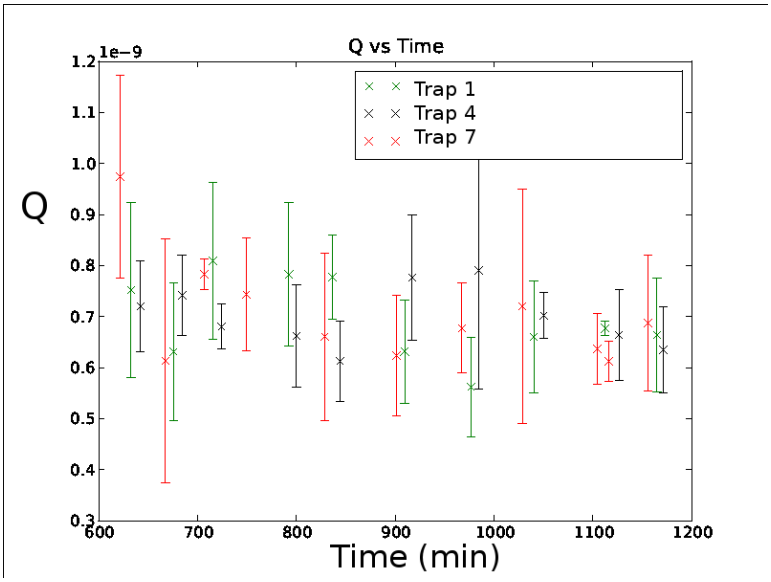

Figure 4.3: Q calculated with the trap depth predicted from the minimization of equation 4.6 is plotted for a particular data set (taken Feb 18, 2011). The roughly constant nature of the value for multiple measurements throughout the day points to a validation of the Reif model.

Chapter 5

Results

5.1 Comparison of $< \sigma v >$ between ^{85}Rb , ^{87}Rb and theoretical predictions

With knowledge of the fact that

$$\Gamma = n_{Rb} < \sigma v >_{Total} + b \tag{5.1}$$

(where b is a background term accounting for residual unwanted gases and 2-body losses) and in order to incorporate dependence of the excited state fraction, we write

$$\Gamma = n_{Rb}(f_e < \sigma v >_e + (1 - f_e) < \sigma v >_g) + b \tag{5.2}$$

where f_e is the fraction of the atoms in an excited state, $< \sigma v >_e$ is the cross section for interactions between excited and ground state atoms, and where $< \sigma v >_g$ is the cross section for interactions between only ground state atoms.

Since the excited state fraction is calculable via equation 2.3 past work within our lab [5] has attempted to predict the values for $< \sigma v >_e$ and $< \sigma v >_g$ based on the method of [7] and the predicted total cross section in equation 5.2 to the measured one, which takes the form of equation 5.1. That is, for our predicted values of $< \sigma v >_e$ and $< \sigma v >_g$, and using our calculable f_e, does $f_e < \sigma v >_e + (1 - f_e) < \sigma v >_g$ match our measured value for $< \sigma v >_{Total}$? The results of such a computation can be seen in figure 5.1.

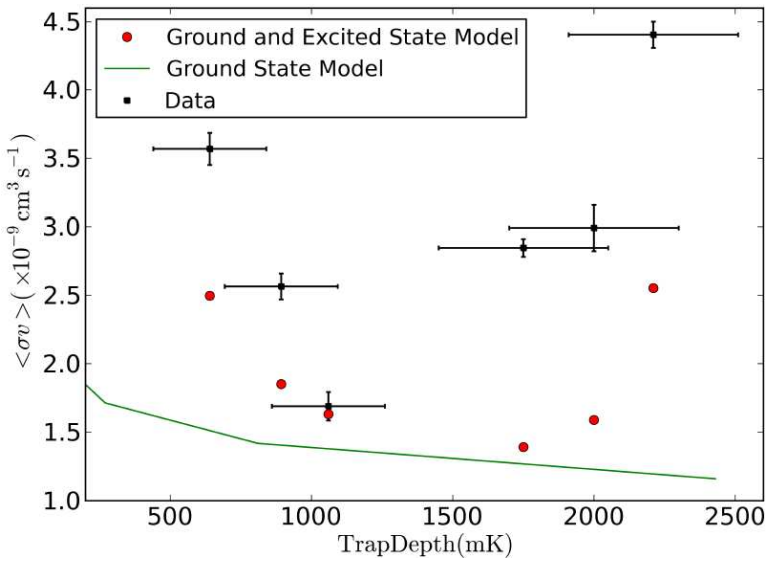

Figure 5.1: A plot comparing the predicted total cross section based on equation 5.2 (red dots) with the measured cross section as in equation 5.1 (black squares). The pure ground state model is also plotted in green [5]

The model presented by equation 5.2 and tested in figure 5.1 is able to reproduce the same shape, or trend, displayed by the data, yet fails to agree within experimental error, and still appears to be systematically different from the measured result. But in spite of the overall failure to predict our data, we are assured that the excited state fraction is an important quanity to be considered when attempting to understand the fundamental nature of cross sections for trap loss. The following paragraphs will, outline possible flaws with this model while the next section will outline an alternative one.

Complicating the jump from equation 5.1 to equation 5.2 is the fact that our background Rubidium gas is actually approximately 2/3 ^{85}Rb and 1/3 ^{87}Rb. The differences in atomic interactions, and thus cross sections, between ground state ^{85}Rb and ground state ^{87}Rb, ground state ^{85}Rb and excited state ^{87}Rb and excited state ^{85}Rb and ground state ^{87}Rb have been ignored on the assumption that most of the interactions result from the outer electrons which are not much effected by the slightly different nucleus of each isotope.

Further, while equation 5.2 considers interactions between "isotope-general" ground and excited states, it does not consider interactions resulting between two excited state atoms. Such contributions would have to consider that the probability for two excited state atoms interacting would go like f_e^2 which is typically at least an order of magnitude less than the corresponding probability for ground-excited state interactions $f_e(1 - f_e)$.

However, since our results are not conclusive, both of these simplifications may have to be revisited in the future in order to explain our results.

Another assumption inherent in the model is that, while we trap one isotope of Rubidium, our lasers to not excite any significant fraction of the other, untrapped isotope. Since the difference between resonant frequencies (ω) for each isotope is

$$\Delta\omega_{85-87} = \omega_{85} - \omega_{87} \simeq 1.126\,\text{GHz} \tag{5.3}$$

we can relate the detunings for each isotope by $\delta_{85} = \delta_{87} - 1.126$ GHz. Typical detunings for magneto-optical traps are 1 - 10 MHz, about two or three orders of magnitude less than the unintentional detuning which acts on the untrapped isotope.

A typical excited state fraction for such a detuning is $\simeq 10^{-5}$, significantly less than the $\simeq 10^{-1}$ excited state fraction of the intentionally trapped isotope.

So though unintentional excitation of the untrapped isotope seems negligible based on the relatively large difference between their resonant excitation frequencies, this large difference actually provides a method for direct measurement of the differently trapped species. If light from fluorescent atoms is first passed through a bandpass filter centred on the resonance of the correct isotope, information about the trapping of each isotope could be recorded independently of the overall florescence signal resulting from the MOT.

5.2 $< \sigma v >$ dependence on the excited state fraction

Considering the strong trend present in figure 5.1, we plot the cross section versus the excited state fraction ($< \sigma v >$ versus f_e) and attempt to infer a relation. Figure 5.2 shows a plot of cross section versus the excited state fraction where an almost linear dependance is observed.

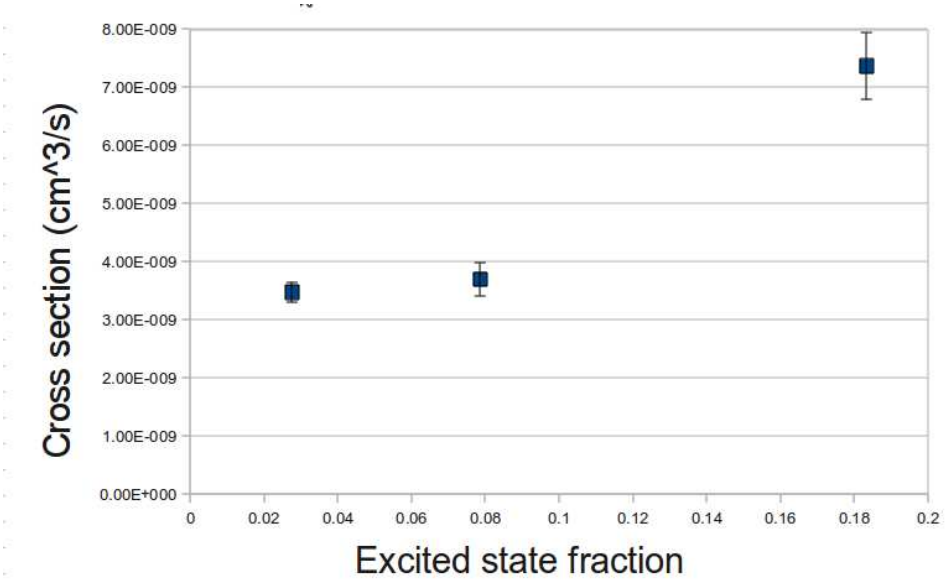

Figure 5.2: $< \sigma v >$ versus f_e for Traps 1, 4 and 7 in table 3.1.

If there was such a simple linear dependence of the cross section on the excited state fraction, then we would be forced to look at modes of trap loss which are related to these types of atoms. Inelastic collisions (some of which are outlined in section 2.5.2) would be prime candidates for this mechanism because they allow for the excess energy in the excited state to be transformed into a kinetic energy that is typically far in excess of any trap depth which our lasers and magnetic fields are able to produce. Since we expect the number of fine structure changing collisions and/or radiative escape occurrences to be directly related to the number of atoms in the excited state, we infer that if these mechanisms are significant modes for trap loss, there should be a dependence of cross section on excited state fraction.

Why don't we put a filter on the photodiode that only passes the frequency mapping to the $P_{3/2} \rightarrow P_{1/2}$ transition? Wouldn't this show if there was a significant amount of FCC collisions going on?

In order to test weather the cross section was indeed solely dependent on the excited state fraction, we measured the cross sections for two pairs of two MOTs each having the same excited state fraction. The summary of these MOTs and their parameters are shown in table 5.1

Trap #	Detuning δ (MHz)	AOM setting	Intensity (mW/cm^2)	Trap Depth (K)	Excited State Fraction	$< \sigma v >$ 10^{-9} cm^3/s
9	12.69	0.7	30.8	?	0.15	9.96 ± 1.12
10	5.56	0.3	7.3	?	0.15	4.83 ± 1.62
11	11.21	0.4	16.1	?	0.11	3.37 ± 1.02
12	15.47	0.6	29.7	?	0.11	8.81 ± 1.16

Table 5.1: A summary of MOT settings and the corresponding excited state fractions for each. There are two pairs of different excited state fractions over four traps of different parameters. The idea is to test whether these different MOTs have the same cross section as a result of having the same excited state fraction.

When cross sections for the traps in table 5.1 are measured and included in a plot like that of figure 5.2 we observe even more puzzling behaviour (see figure 5.3).

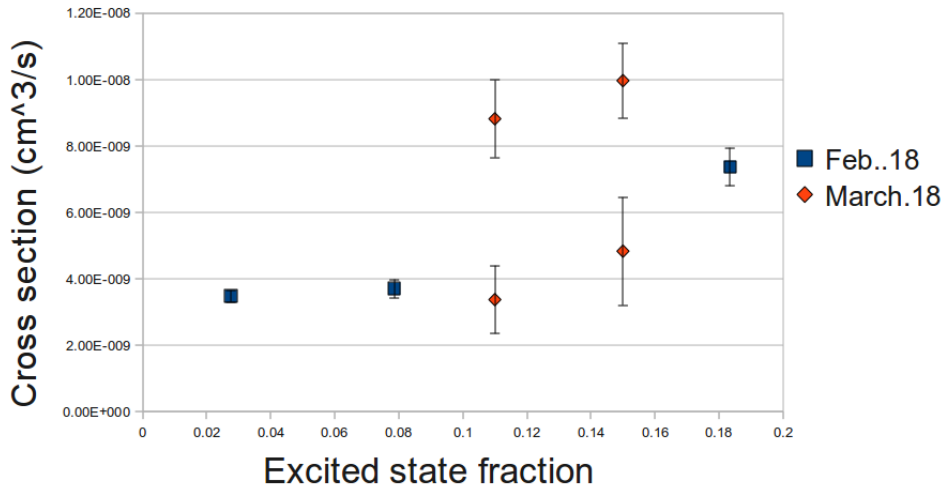

Figure 5.3: $< \sigma v >$ versus f_e for Traps 1, 4 and 7 in table 3.1 (Blue) as well as all the traps in table 5.1. The red dots are the results for the traps in table 5.1.

If one could imagine anyway in which the system had directionality - some way in which these MOTs traversed the excited state fraction space - then figure 5.3 might appear to exhibit a hysteresis. However, given that the next section is devoted entirely to data quality issues, I won't speculate any farther possible relations between the excited state fraction and the cross section for trap loss.

5.3 Data quality issues: different $< \sigma v >$ measurements for the same trap

Having measured the cross section for all traps in tables 3.1 and 5.1, we can add these results to plots like those of figures 5.3 and 5.1. Figures 5.4 and 5.5 plot $< \sigma v >$ versus trap depth for multiple traps containing either ^{85}Rb or ^{87}Rb. Immediately these plots tell us that, while we are still observing the anomalous behaviour which disagrees with our current model, we are not able to obtain reproducible results. A new measurement of the same quantity for the same trap sometimes yields different results.

This failure to obtain reproducible results also inhibits the analysis of section 5.2. If one adds all the data in figure 5.4 to a plot of the cross section versus the excited state fraction, the possible linear relation that looked so hopeful in figure 5.2 becomes rather an eyesore (see figure 5.6).

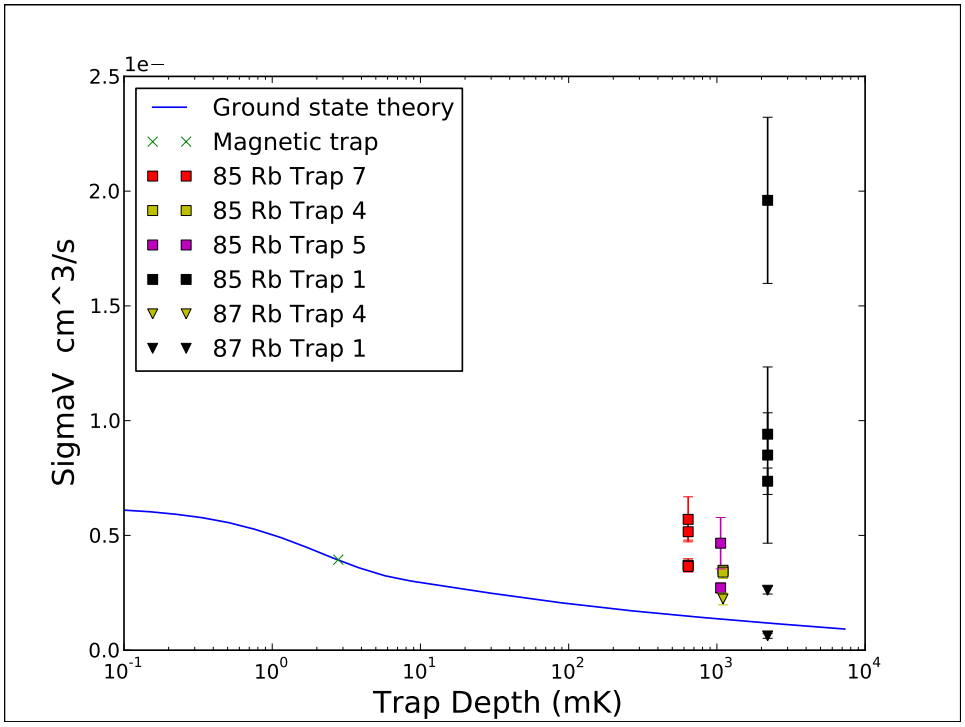

Figure 5.4: $< \sigma v >$ versus Trap depth (U) for the traps in table 3.1. The same measurement of the same trap was taken on different days and sometimes produced different results. Measurements of the same trap appear in the same colour. The measurements of traps for ^{85}Rb are in squares , while ^{87}Rb uses triangles.

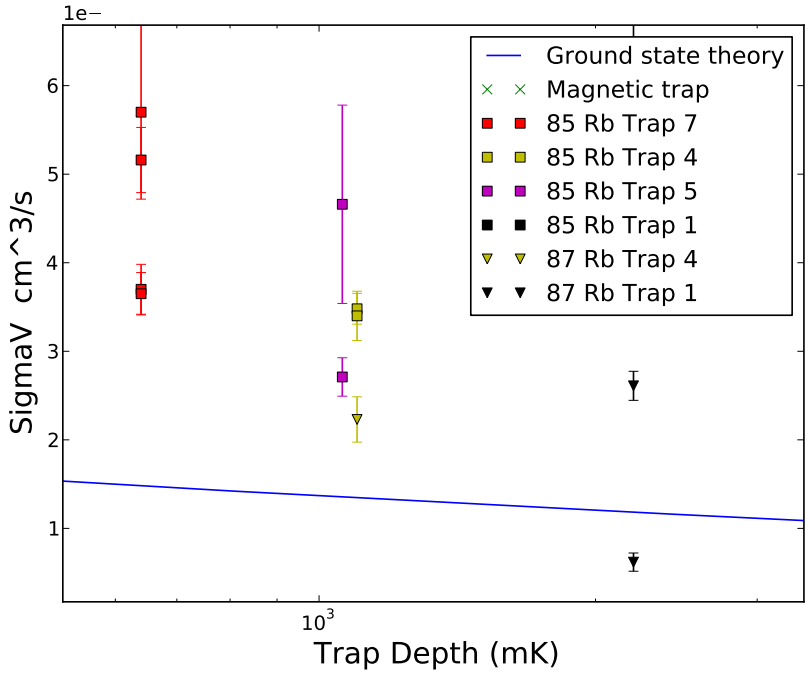

Figure 5.5: $< \sigma v >$ versus Trap depth (U) for some of the traps in table 3.1. The same measurement of the same trap was taken on different days and sometimes produced different results. Measurements of the same trap appear in the same colour. The measurements of traps for ^{85}Rb are in squares , while ^{87}Rb uses triangles.

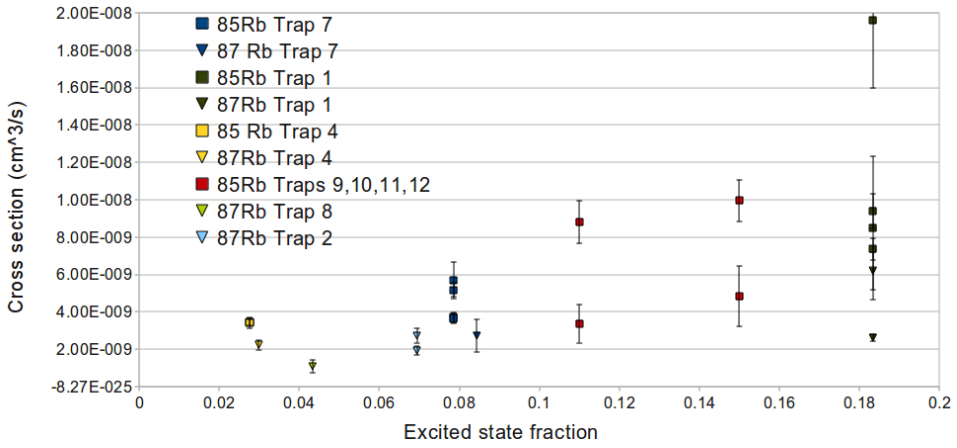

Figure 5.6: $< \sigma v >$ versus exited state fraction (f_e) for the traps in tables 3.1 and 5.1. The same measurement of the same trap was taken on different days and sometimes produced different results. Measurements of the same trap appear in the same colour. The measurements of traps for ^{85}Rb are in squares , while ^{87}Rb uses triangles.

So it is clear that before a concrete quantification of the dependence of the cross section on the excited state fraction can be made, the experimental procedure, set up, or data analysis must be altered or at least better understood so that we can be certain our measurements are correct and reproducible.

Chapter 6

Conclusions

6.1 The Reif Model and Trap Depth predictions

We have produced experimental evidence that verifies the Reif model. The constant nature of equation 6.1

$$Q = \frac{R}{U^2 n_{Rb}} = \frac{2A}{\pi m_{Rb}^2 v_T^2} \tag{6.1}$$

for different trap depths (U) across different density regimes (n_{Rb}) is displayed in figures 4.2 and 4.3.

The model has allowed us to turn the determination of the trap depth into a simple minimization problem. Since we have measured the trap depths independently, a correction for the determination of trap depth with v_c, the capture velocity, instead of the more accurate escape velocity, v_e can also be made. We determine this correction factor to be $k = 1.1 \pm 0.45$ (see equation 4.7), and note that it should be included when attempting to measure trap depth, as well as monitored for verification.

The Reif model and the presented method for measuring trap depth can be strained in the following ways:

- Misalignment of the lasers: If the lasers are realigned between measurements of R, n_{Rb} and possibly trap depth (U), then our assumption that $\Delta A \simeq 0$ may break the constant nature of Q. If this were the case we will be forced to consider a dependence of R or U on the laser alignment. If there was such a dependence, this might explain the large scatter in our data for measurements of cross sections for trap loss ($< \sigma v >$).

- Drive the Reif Model to extreme Regimes: If we take our traps to either very high or low regimes of density, n_{Rb}; load rate ,R; Trap depth, U; or temperature, T (remember $v_T = \sqrt{\frac{8k_B T}{\pi m}}$); we can put the Reif Model under greater scrutiny. It would be very interesting to find a regime where the model *broke*.

Future work should consider re-measureing trap depths for those traps in table 3.1 and attempting to confirm the viability of the presented method. This method would also allow us to take data for both the cross section, $< \sigma v >$, and Trap depth, U, in order to populate $< \sigma v >$ vs U curves like in figures 1.5 and 1.6. More data points would help better map the parameter space and either confirm the theoretical curve or provide more distinct structure to the disagreement.

6.2 Speculations on the cross section for trap loss, $< \sigma v >$

We see a disagreement from theoretical predictions of the cross section for trap loss (see figure 1.6), and a strong correlation between the cross section and the excited state fraction of the trapped atom population (figures 5.6 5.1). In order to quantify this more concretely future work must be able to obtain reproducible data.

Possible sources of error that might result in different measurements of the same cross section include laser alignment as well as our model of the scattering rate (equation 3.1). As previously mentioned, aligning the lasers slightly differently for each data run may effect the cross-sectional area of the trap A, the loading rate R, or even the trap depth U, any of which would certainly change our measurement of $< \sigma v >$.

The scattering rate is derived from a two level atomic model yet Rubidium atoms are multi-levelled. Instead of normalizing equation 3.1 to the scattering rate, we might instead normalize to the atomic florescence of some standard MOT. Calculation of the number of trapped atoms would then become a relative quantity. However, if the two level model is insufficient, the scattering rate normalization may be wrong to different degrees for different traps - a pitfall we avoid with normalization to a standard MOT florescence.

So addressing these two issues is the next step in obtaining reliable data and quantifying the relation between the cross section ,$< \sigma v >$, and the excited state fraction, f_e.

Bibliography

[1] M. H. Anderson, J. R. Ensher, M. R. Matthews, C. E.Wieman, and E. A. Cornell, 1995, Science 269, 198.

[2] A.V. Andreev (2006). *Atomic Spectroscopy: Introduction to the Theory of Hyperfine Structure*. New York: Springer.

[3] T. Calarco, E. A. Hinds, D. Jaksch, J. Schmiedmayer, J. I. Cirac, and P. Zoller, Phys. Rev. A 61, 022304 (2000).

[4] J. Camparo, Physics Today. 60 ,11 (2007).

[5] D. Clement, (2011) Directed Studies Internal Report. University of British Columbia.

[6] F. Esnault, D. Holleville, N. Rossetto, S. Guerandel, N. Dimarcq, Phys Rev. A 83 033436 (2010).

[7] D. Fagan, (2009) *Study of Collision Cross Section of Ultra-Cold Rubidium using a Magneto-optic and pure Magnetic trap*. Undergraduate Thesis. University of British Columbia.

[8] R. Folman et al., Phys. Rev. Lett. 84, 4749 (2000).

[9] D.J. Griffiths (2005). *Introduction to Quantum Mechanics*. Prentice Hall.

[10] K. Ladouceur, (2008) *Experimental Advances toward a Compact Dual-Species Laser Cooling Apparatus*. Master Thesis. University of British Columbia.

[11] R. Loudon, (1983) *The Quantum Theory of Light*, 2nd ed. Oxford University Press.

[12] H.J. Metcalf, P. Straten, (2002). *Laser Cooling and Trapping*. New York: Springer.

[13] C. Monroe, W. Swann, H. Robinson, C. Wieman, Phys. Rev. Lett. 65, 1571 (1990).

[14] J. Pade, Eur. Phys. J. D 44, 345-350 (2007).

[15] F. Reif (1965). *Fundamentals of Statistical and Thermal Physics*. New York: McGraw-Hill.

[16] D. A. Steck, Rubidium 87 D Line Data, available online at http://steck.us/alkalidata (revision 2.1.2, 12 August 2009).

[17] D. A. Steck, Rubidium 85 D Line Data, available online at http://steck.us/alkalidata (revision 2.1.2, 12 August 2009).

[18] J. Weiner, V. S. Bagnato, S. Zillo, and P. S. Julienne, Rev. Mod. Phys. 71, 1 (1999).

[19] C. Zhu, (2009) *Investigation into Heating and Hyperfine Loss Mechanisms in Magnetically Trapped Ultra-Cold Rubidium*. Undergraduate Thesis. University of British Columbia.

Appendix A

Below are tables outlining the which traps were measured on which dates. In all cases, the experimental method follows that of section 3. Table A.1 represents data taken for this thesis while table A.2 contains data from [5].

Traps	Trapped Rb Isotope	Date
1,2,4	87	October 5, 2010
1,5,7	85	November 4, 2010
1,5,7	85	January 24, 2011
1,4,7	85	February 18, 2011
1,4,7	85	March 7, 2011
8,9,10,11	85	March 18, 2011

Table A.1: Measurements of different traps are displayed according to data and trapped isotope. Trap numbers are from table 3.1

Traps	Trapped Rb Isotope	Date
1,3,4,7	87	July 13, 2010
1,2,8	87	July21, 2010

Table A.2: Measurements of different traps (from [5] are displayed according to data and trapped isotope. Trap numbers are from table 3.1